A Study of the Interaction of the North Atlantic Oscillation with Ocean Circulation

JOHN MARSHALL, HELEN JOHNSON,* AND JASON GOODMAN

Department of Earth, Atmospheric and Planetary Sciences, Massachusetts Institute of Technology, Cambridge, Massachusetts

(Manuscript received 29 August 1999, in final form 3 April 2000)

ABSTRACT

Observed patterns of wind stress curl and air–sea heat flux associated with the North Atlantic oscillation (NAO) are used to discuss the response of ocean gyres and thermohaline circulation to NAO forcing and their possible feedback on the NAO. The observations motivate, and are interpreted in the framework of, a simple mathematical model that couples Ekman layers, ocean gyres, and thermohaline circulation to the atmospheric jet stream. Meridional shifts in the zero wind stress curl line are invoked to drive anomalies in ocean gyres, and north–south dipoles in air–sea flux drive anomalous thermohaline circulation. Both gyres and thermohaline circulation play a role in modulating sea surface temperature anomalies and hence, through air–sea interaction, the overlying jet stream. The model, which can be expressed in the form of a delayed oscillator with ocean gyres and/or thermohaline circulation providing the delay, identifies key nondimensional parameters that control whether the ocean responds passively to NAO forcing or actively couples. It suggests that both thermohaline circulation and ocean gyres can play a role in coupled interactions on decadal timescales.

1. Introduction

The North Atlantic oscillation (NAO) is the primary mode of atmospheric low-frequency variability over the North Atlantic basin and a controlling influence on variability in air–sea interaction. The patterns of air–sea interaction associated with the NAO have a rather robust spatial pattern—see Cayan (1992)—but are largely stochastic in time. The ocean, at least on short timescales, responds passively to this forcing, reddening the essentially white spectrum of imposed variability. The reddening process involves the mixed layer (e.g., Frankignoul and Hasselmann 1977; Battisti et al. 1995; Hall and Manabe 1997; Barsugli and Battisti 1998), Rossby wave propagation (e.g., Frankignoul et al. 1997; Jin 1997; Weng and Neelin 1998; Neelin and Weng 1999; Cessi 2000), mean flow advection (Saravanan and McWilliams 1998), and thermohaline circulation (e.g., Griffies and Tziperman 1995; Delworth and Greatbatch 1999). The relative importance of these reddening mechanisms must depend on timescale, mixed layers dominating on short timescales, and, presumably, ocean gyres and thermohaline circulation increasing in importance as the timescale lengthens. Observationally it is difficult to tease these mechanisms apart. However, low-frequency variability of the interior Atlantic Ocean and its association with the NAO, has now been documented in observations (e.g., Dickson et al. 1996; Curry et al. 1998). The interior ocean clearly reflects the influence of variability in the forcing orchestrated by the NAO.

Observations tell us that in midlatitudes air–sea interaction acts to rather strongly damp SST and associated oceanic thermal anomalies generated by stochastic atmospheric forcing (see, e.g., Frankignoul et al. 1998), but of great interest is the possibility that advection of heat by ocean circulation might offset local damping of SST by air–sea interaction, making possible oscillatory modes of approximately decadal period, rather than strongly damped ones. These, through their effect on SST, could then imprint themselves back on the atmosphere and so modulate the amplitude and phase of the NAO (see, e.g., Rodwell et al. 1999) on longer timescales. There is a suggestion of covarying patterns of atmospheric and oceanic variability in the observations analyzed by Deser and Blackmon (1993) and Sutton and Allen (1997). Furthermore, analysis of coupled atmosphere–ocean models (Grotzner et al. 1998; Timmerman et al. 1998; Selten et al. 1999) suggest that the ocean can indeed modulate the spectrum of variability in the overlying atmosphere. But it is not yet clear to what extent the interaction between the two fluids in the Atlantic is a truly coupled one (see Delworth and Great-

* Current affiliation: Department of Meteorology, University of Reading, Reading, United Kingdom.

Corresponding author address: Dr. John Marshall, Earth, Atmospheric and Planetary Sciences, MIT, 77 Massachusetts Ave., Bldg. 54-1526, The Green Building, Cambridge, MA 02139-4307.
E-mail: marshall@gulf.mit.edu

batch 2000). The atmosphere may respond ''passively'' to SST anomalies on longer timescales, feeling the ''imprint'' of ocean circulation and having its spectra reddened by it (e.g., Jin 1997; Weng and Neelin 1998). An ''active'' coupling involving feedback between the midlatitude atmosphere and ocean is also possible involving gyre dynamics (e.g., Latif and Barnett 1994; Jin 1997; Goodman and Marshall 1999; Cessi 2000) and/or thermohaline circulation (Hakkinen 2000). A useful brief review of prototype models of atmosphere–ocean interaction in midlatitudes is given in the introduction of Neelin and Weng (1999).

The extent to which the interaction between the NAO is one way (NAO driving ocean) or two way (feedback of SST on the NAO) remains unclear. A major complicating factor is the apparent lack of a robust and consistent response in atmospheric models, and perhaps of the atmosphere too, to midlatitude SST anomalies (Palmer and Sun 1985; Peng et al. 1997; Kushnir and Held 1996). Recently it has been shown (see Rodwell et al. 1999; Mehta et al. 2000) that SST anomalies may influence the phase of the NAO at low frequencies in atmospheric models driven by observed SST anomalies. As discussed in Bretherton and Battisti (2000), however, these modeling results can be understood in terms of the passive response of the ocean to atmospheric forcing, with atmospheric temperatures and SST equilibrating toward one another at low frequencies. However, if changes in ocean circulation induced by NAO forcing play a role in modulating SST anomalies on longer timescales, then, to the extent that the atmospheric temperatures and SST covary at low frequencies, the effect of ocean advection may imprint itself on the atmosphere (see Czaja and Marshall 2000).

The goal of the present study is to develop a theoretical framework in which we can explore the nature of NAO–ocean interactions. The model sets up in a transparent way the interplay of local air–sea interaction and anomalous advection of heat by Ekman layers, ocean gyres, and thermohaline circulation in setting SST anomalies, the possible effect of those anomalies on the overlying wind patterns, and their feedback on ocean circulation. The danger of such an approach, of course, is that for such models to be amenable to analysis, of necessity they have to be rather simple. And that simplicity, although attractive, can lead to the theoretical construct becoming quickly irrelevant to the real problem at hand. We have therefore striven hard to develop a framework that is strongly motivated by, and has strong contact points with, observations.

In section 2 we spend some time inspecting observed patterns of wind stress curl and air–sea heat flux associated with the NAO and use them to discuss the dynamical response of ocean gyres and thermohaline circulation to NAO forcing. We introduce the idea of an ''intergyre'' gyre, a gyre anomaly that straddles the climatological confluence of the subtropical and subpolar gyres and is driven by meridional shifts in the wind pattern. On decadal timescales the intergyre gyre controls the transfer of heat and fluid properties across the climatological windstress curl line, from one side of the atmospheric jet stream to the other. When the NAO is positive (negative) the zero wind curl line is poleward (equatorward) of its climatological position, the intergyre gyre is anticyclonic (cyclonic), and the trajectory of the North Atlantic Current is more poleward (zonal) than in the mean and carries more (less) heat meridionally. As described in section 3, our underlying conceptual model has been very much influenced by the seminal study of Atlantic air–sea interaction by Bjerknes (1964), who suggested that such changes in meridional heat transport in the ocean would be compensated by changes in atmospheric heat transport, in such a way that the heat carried by the two fluids together would remain constant. Indeed the present study could be regarded as a theoretical exposition of some of the major themes set out in Bjerknes (1964). The coupled model itself is summarized in section 3; a detailed account of its derivation can be found in the appendix. The model addresses those processes that can influence upper-ocean thermal properties and SST anomalies in the region of the separated Gulf Stream, to which the atmospheric storm track is likely to be sensitive. Properties of the model, which can be expressed as a delayed oscillator, with gyres and/or thermohaline circulation providing the delay, are analyzed in section 4. Key nondimensional parameters are identified that control the nature of the interaction and whether the coupling is active or passive. We believe these parameters have an importance that transcends the simple model used to identify them. In section 5, we discuss the implications of our study for NAO–ocean interactions.

2. The response of the ocean to NAO forcing

a. Patterns of air–sea interaction

The climatological position of the annual-mean zero-wind-stress-curl line over the North Atlantic exhibits a pronounced tilt, from SW to NE, as shown in Fig. 1a. To its north the windcurl is positive, driving the cyclonic subpolar ocean gyre; to its south it is negative driving the anticyclonic subtropical gyre. The line marks the confluence of the two gyres where the Gulf Stream turns eastward in to the interior of the ocean and feeds the North Atlantic Current. Figure 1b plots the anomaly in windstress curl associated with the NAO during December–February (DJF).[1] It is important to note that the anomaly is not merely a waxing and waning of the

[1] The NAO anomaly fields discussed here were computed by regressing NCEP–NCAR reanalysis (1958–98) fields onto the winter-mean (DJF) NAO index of Hurrell (1995). They correspond to a (Hurrell) NAO index of +1 (See Visbeck et al. 1998).

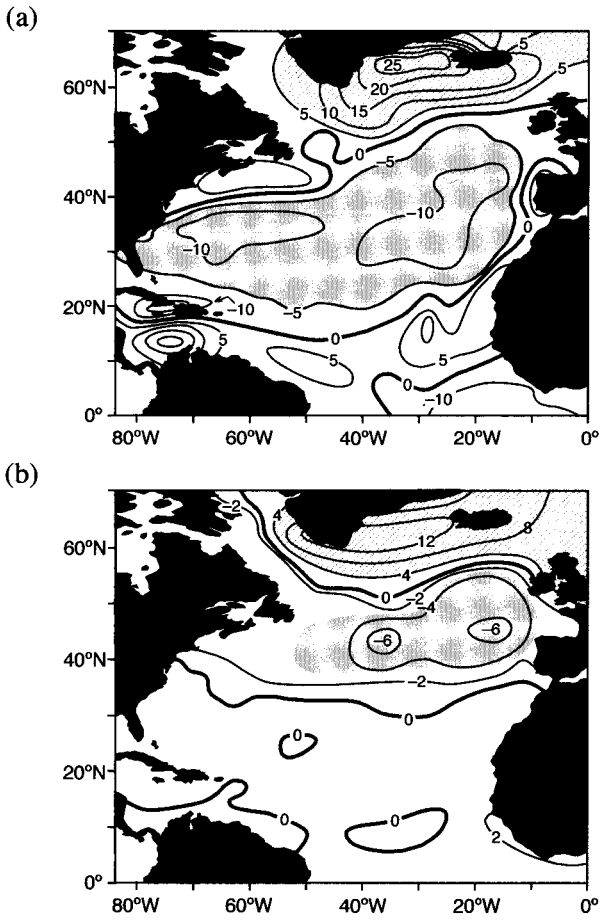

FIG. 1. (a) Annual-mean wind stress curl over the North Atlantic in units of 10^{-8} N m^{-3}—anticyclonic regions are stippled, cyclonic regions are hatched. The zero wind curl lines are indicated by the thick black line; (b) the anomaly in wind stress curl associated with the NAO(+) in the same units.

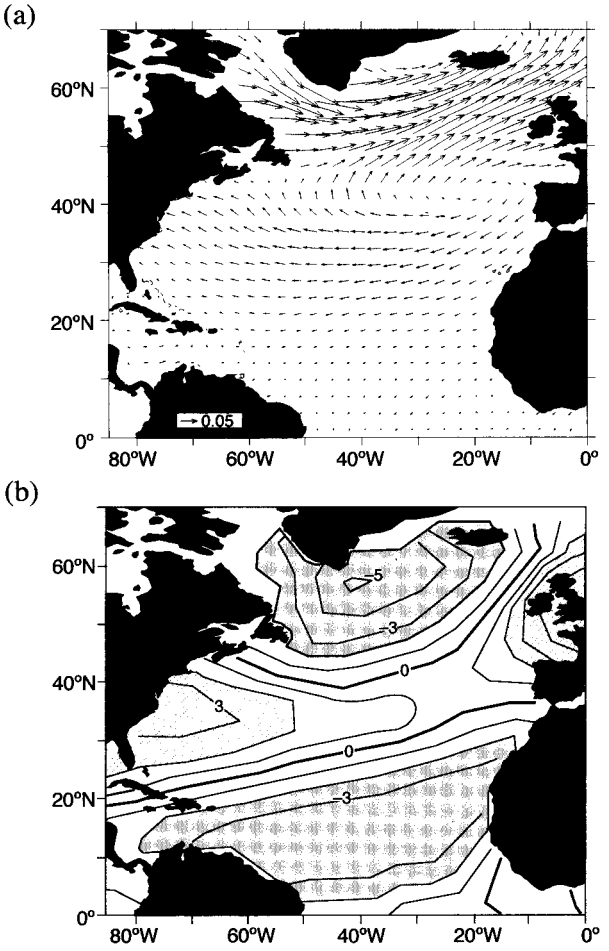

FIG. 2. (a) The anomaly in surface wind stress associated with NAO(+). The arrow scale represents a stress of 0.05 N m^{-2}. (b) The pattern of SST anomalies that regress onto the NAO(+)—contour interval 1/10 K.

climatological pattern. The zero-curl lines of the anomaly have a more zonal orientation than that of the mean zero-curl line and are shifted significantly poleward. It is better to think of the anomaly as a *shift* in the mean pattern rather than just a modulation in its strength: on adding the anomaly to the mean (NAO+) the zero-curl line has a more pronounced tilt, on subtracting it (NAO−) the line is more zonal. This is entirely consistent with Rogers (1990), who observed that during high NAO months, storms track along a more pronounced SW to NE path and so the Icelandic Low, the ''graveyard'' of depressions at the end of the Atlantic storm track, is enhanced in strength. In low NAO months, however, storms have a much more zonal path and the Icelandic low is weaker. Figure 2a shows the anomaly of surface stress associated with NAO(+), whose curl yields Fig. 1b. The pronounced poleward shift of the anomaly in eastward stress, reaching a maximum of 0.1 N m^{-2} at ~60°N, is very evident. This north–south migration of the jet stream as the NAO rises and falls will be a central element of the coupled model discussed in section 3.

Significant changes in air–sea heat fluxes and Ekman transport accompany these changes in the wind. Figure 3a plots the anomalous (latent plus sensible) heat fluxes associated with the NAO; we observe the characteristic pattern discussed in Cayan (1992). When the NAO is high there is enhanced cooling of the ocean poleward of 45°N inducing negative SST anomalies there and diminished air–sea fluxes between 30° and 45°N, inducing positive SST anomalies—See Fig. 2b. This dipole pattern in air–sea flux, shaded in Fig. 3a for emphasis, straddles the climatological position of the zero wind curl line (see Fig. 1a).

Before going on we should emphasize that these patterns of variability in air–sea interaction are rather robust in space but are stochastic in time, being driven primarily by synoptic-scale variability internal to the atmosphere that is essentially uncorrelated on timescales longer than 1 month and so has a ''white'' spectrum.

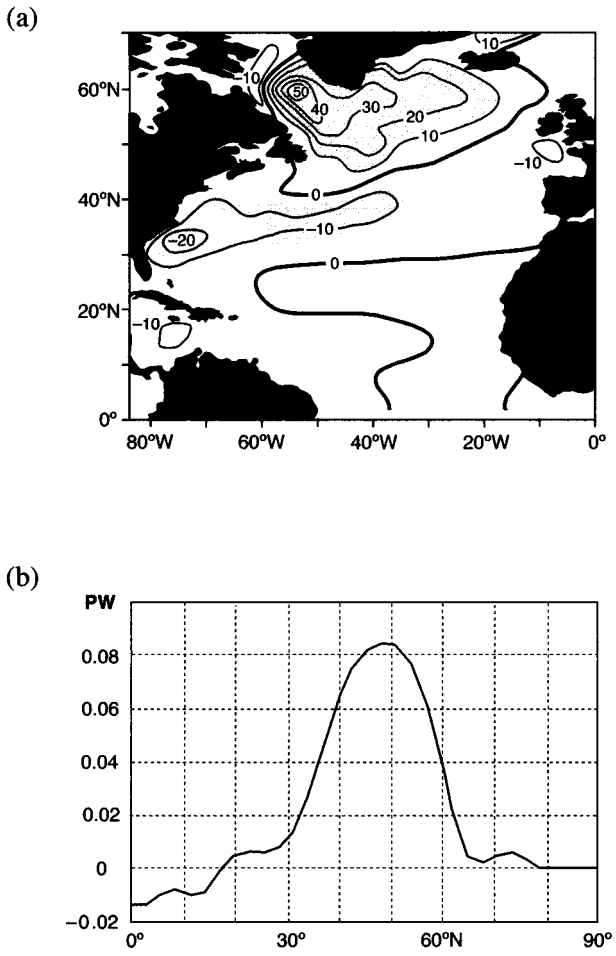

FIG. 3. (a) The pattern of anomalous (latent + sensible) heat fluxes associated with NAO(+) (W m^{-2}). Positive fluxes are directed out of the ocean. (b) The implied anomaly in meridional oceanic heat transport (PW = 10^{15} W) obtained by integrating the pattern in Fig. 3a zonally across the basin and then summing meridionally.

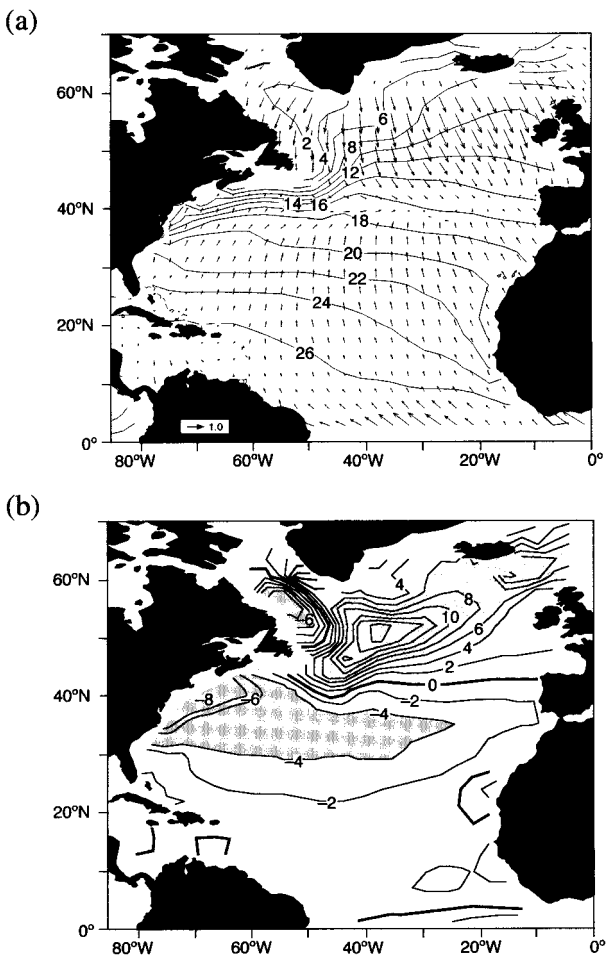

FIG. 4. (a) Ekman transport (m^2 s^{-1}) associated with NAO(+) superimposed on DJF SST climatology. (b) Pseudo air–sea Ekman heat flux (W m^{-2}) associated with NAO(+), computed from Eq. (1) using the data shown in Fig. 4a. Positive fluxes are directed out of the ocean.

However, because of its great thermal and dynamical inertia, the ocean responds with greater power at low frequencies providing a reddening mechanism.

b. Ekman transport

The Ekman transport is plotted in Fig. 4a superimposed on the DJF mean SST. It is southward to the north and northward to the south. Thus in NAO(+) the Ekman layers advect cold water from the north and warm water from the south. In Fig. 4b the Ekman heat transport is expressed as a pseudo air–sea heat flux,

$$H_{\text{ek}} = c_o \mathbf{M}_{\text{ek}} \cdot \nabla \text{SST}, \tag{1}$$

where c_o is the specific heat of water, $\mathbf{M}_{\text{ek}} = -\mathbf{k} \times \boldsymbol{\tau}_{\text{NAO}}/f_o$ is the transport of the Ekman layer with $\mathbf{k}$ a unit vector in the vertical, $\boldsymbol{\tau}_{\text{NAO}}$ is the wind stress associated with the NAO plotted in Fig. 2a, and f_o is the Coriolis parameter. We see that H_{ek} induces cooling to the north and warming to the south of magnitude, which can reach several tens of watts per square meter. On short timescales $\mathbf{M}_{\text{ek}}$, and hence H_{ek}, will be dominated by imposed synoptic-scale variability. But if dipole SST anomalies straddling the Gulf Stream, with cold to the north and warm to south, reinforce the NAO(+), as one might expect, then the pattern H_{ek} could act as a positive feedback on SST, keeping cold SST cold and warm SST warm. This will be an important element of the model developed in section 4 and is observed in experiments with atmospheric GCMs (AGCMS; see Palmer and Sun 1985; Rodwell et al. 1999).

c. The intergyre gyre

What is the response of the ocean to these anomalous forcing patterns? It is shown in Battisti et al. (1995) that SST variability on interannual timescales over the Atlantic can be understood in terms of one-dimensional

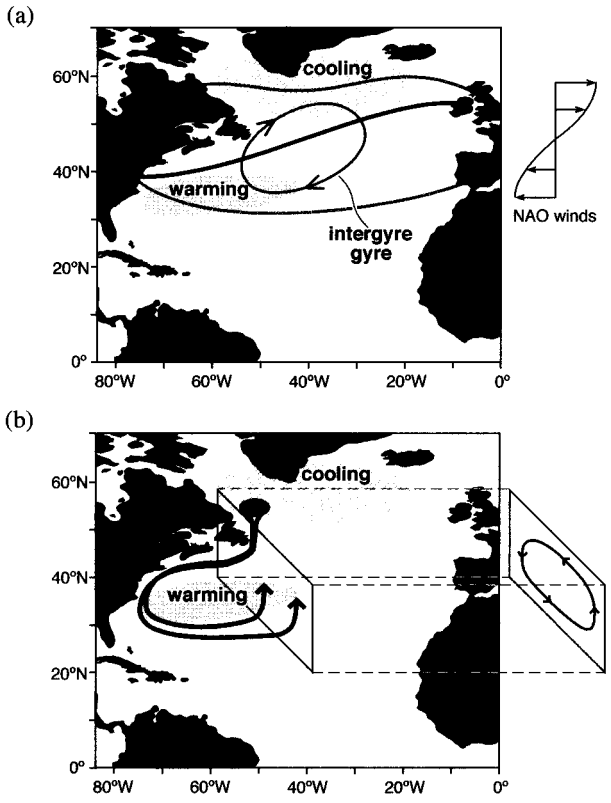

FIG. 5. (a) Schematic diagram showing the Z whose diagonal is the zero wind curl line of the climatology (Fig. 1a) and whose top and bottom are the zero wind curl lines of the NAO anomaly (Fig. 1b). Regions of warming and cooling of the ocean due to the air–sea flux anomalies shown in Fig. 3a are indicated. The sense of the intergyre gyre spun up by NAO(+) wind curl forcing is also shown. (b) Schematic diagram of the anomaly in thermohaline circulation induced by the dipole in ocean thermal anomalies created by anomalies in air–sea heat fluxes associated with NAO(+) shown in Fig. 3a. The overturning circulation sketched in the meridional section on the right represents a zonal average picture.

mixed layer processes, except in the region of the separated Gulf Stream where advection by ocean currents are hypothesized to play a role. Indeed in regions of swift currents advective heat transport by ocean circulation is likely to play an important role on decadal timescales, because they are associated with such large heat transports. Observations of the possible influence of ocean dynamics on SST patterns on decadal timescales is given, for example, by Bjerknes (1964), Hansen and Bezdek (1996), and Sutton and Allen (1996). Luksch (1996) shows that advection of heat by ocean currents can be comparable to that due to air–sea heat fluxes, particularly in the region of the separated Gulf Stream. Halliwell (1998) also shows convincing evidence of a geostrophic modulation of SST anomalies in the Gulf Stream region.

The patterns of air–sea interaction described above suggest the following simple schematic of upper-ocean response to NAO forcing, sketched in Fig. 5. We draw a ''Z,'' its diagonal marking the position of the tilted climatological wind stress curl line (Fig. 1a), its top and bottom marking the position of the horizontal zero-curl lines of the anomaly (Fig. 1b). The tilted diagonal is coincident with the climatological position of the seaward extension of the Gulf Stream/North Atlantic Current, separating the subpolar and subtropical gyres. The NAO wind curl anomaly is, at any instant, of uniform sign between the top and bottom of the Z, but is stochastic in time. This temporally stochastic but spatially coherent forcing pattern drives, we imagine, a circulation anomaly that crosses from one gyre to the other. We will call this anomalous circulation pattern the ''intergyre'' gyre, which we represent by its transport streamfunction Ψ_{ig}. The transport of the intergyre gyre is the value of this streamfunction just inside the western boundary current, which we represent thus: $\Psi_{ig|w}$. Because the baroclinic modes in the ocean can respond only at low frequencies, the sign of the intergyre gyre will fluctuate in time, but at much lower frequencies than that of the imposed forcing, thus providing a reddening mechanism.

A stochastic Rossby wave model of the intergyre gyre will be presented in section 4, in which the reddening process is the finite time required for Rossby waves to propagate across the basin. We will see in a moment that significant ocean heat flux anomalies are associated with Ψ_{ig} and so it is likely to play an active role in the evolution of SST anomalies. Moreover, the sense of the intergyre circulation and heat anomaly can remain of one sign for decades. If it were consistently anticyclonic, for example, then adding it to the mean would indicate that the path of the North Atlantic Current has been displaced poleward of its climatological position, keeping more northerly latitudes warmer. Conversely, in the opposite phase, the North Atlantic Current would be more zonal and supply of heat to more northerly latitudes would be anomalously low. This was precisely one of the conjectures made by Bjerknes (1964) in discussing changes in ocean circulation induced by shifts in the strength and position of the Icelandic low.[2] He argued, invoking Sverdrup (1947), that in periods when the Icelandic low was anomalously deep (shallow), the North Atlantic Current would have a more poleward (zonal) trajectory. As yet, however, there is no incontrovertible observational evidence to support these ideas. Taylor and Stephens (1998) present observations of Gulf Stream position that suggest that it is indeed a delayed response to NAO forcing, much as conjectured by Bjerknes (1964) and as is assumed in this study. However, Joyce et al. (2000) use a different metric of Gulf Stream position and find that it indeed covaries with the NAO but with zero time lag.

[2] Bjerknes (1964) did not use the term NAO. But he did couch his discussion in terms of the strength and position of the Icelandic low, which he argued was sensitive to the ''zonal index'' of Rossby (1939).

HEAT TRANSPORT OF INTERGYRE GYRE

Let us now consider the heat-flux anomalies associated with the NAO and associated SST tendencies. The shaded regions in Fig. 5a represent the dipole anomaly in air–sea heat flux, a schematic representation of the pattern observed in Fig. 3a. During NAO(+) the (anomalous) air–sea heat flux is positive (out of the ocean) to the north and negative to the south, reaching magnitudes of many tens of watts per square meter. If such anomalies were sustained for many years, very large thermal and SST fluctuations would be induced. For example a heat flux anomaly of only 10 W m^{-2} can warm a 100-m layer of ocean by ~7°C in a decade. Observed midlatitude SST anomalies are much less than this, rarely exceeding ±1°C. Clearly on these long timescales some process must balance SST tendencies induced by air–sea interaction. Anomalous advection of heat by ocean circulation must play this role.

One can compute the anomalous meridional ocean heat flux that would be required to *completely* balance the air–sea flux anomaly. This ''implied'' ocean heat flux, obtained by integrating the surface flux pattern in Fig. 3a zonally across the basin and then summing meridionally, is plotted in Fig. 3b.[3] It has a maximum of 0.08 PW at 48°N, at the boundary of the two gyres, where the intergyre gyre has its maximum amplitude. In fact, as sketched in Fig. 5a, the sense of the intergyre gyre is just that which is required to offset changes in SST induced by air–sea heat flux anomalies associated with NAO(+). When the intergyre gyre is circulating anticyclonically it carries heat poleward across the tilted zero-wind-stress-curl line, from the anomalous patch of warming to the south to the anomalous patch of cooling to the north. Heat is carried in the opposite direction when the gyre circulates cyclonically under NAO(−) forcing, but again from regions of warming to cooling. If $\Psi_{ig|w}$ is the strength of the intergyre (in Sv; Sv $\equiv 10^6$ m^3 s^{-1}) then its heat transport across the zero curl line, Q_{ig}, can be estimated as follows:

$$Q_{ig} = \rho_o c_o \overline{\Delta T}^{\text{zero curl}} \Psi_{ig|w}, \tag{2}$$

where ρ_o is the density of water, c_o is its specific heat, $\Psi_{ig|w}$ is the transport of the gyre (evaluated just inside the western boundary current), and $\overline{\Delta T}^{\text{zerocurl}}$ is the change in the mean SST along the climatological position of the mean zero curl line. If $\overline{\Delta T}^{\text{zerocurl}} = 6$°C (corresponding to a cooling moving along the mean path of the North Atlantic Current—see mean SST contours plotted in Fig. 4a), then $Q_{ig} \sim \pm 0.07$ PW if $\Psi_{ig|w} = \pm 3$ Sv. Thus the intergyre gyre can supply the implied ocean heat flux plotted in Fig. 3b if it fluctuates in strength by only a few Sverdrups. It is also important to remember that such anomalies are induced by changes in the strength of ocean gyres, which can be maintained for decades, because that is the inherent timescale over which $\Psi_{ig|w}$ varies. They can thus be expected to play a key role on decadal timescales.

d. Thermohaline circulation

It is known that the NAO is an important modulator of convective activity at deep convection sites in the North Atlantic, and particularly the Labrador Sea (see Dickson et al. 1996; Lab Sea Group 1998). Direct observations of the overturning circulation are not available but models show that the thermohaline circulation is sensitive to dipole NAO forcing (Delworth and Greatbatch 2000). When the NAO is strong, cooling of the polar oceans is enhanced (see Fig. 3a). Should this cooling persist then one might expect the vigor of the meridional overturning to increase, and hence also its associated poleward heat transport. If Ψ_{moc} is the anomaly in the overturning stream function and $\overline{\Delta T}^z$ is the difference in the mean temperature over its vertical extent, then its horizontal heat transport is

$$Q_{moc} = \rho_o c_o \overline{\Delta T}^z \Psi_{moc}. \tag{3}$$

In the mean the thermohaline circulation of the Atlantic Ocean has a strength of ~20 Sv and carries in excess of 1/2 PW of heat poleward at 40°N. Thus fluctuations of 1/10 PW can be achieved if the overturning circulation changes in strength by only 20%, or $\Psi_{moc} = \pm 4$ Sv.

Figure 5b plots a schematic of the imagined anomaly in thermohaline circulation induced by the NAO(+) buoyancy anomalies. Note that the lateral scale of the anomalous overturning is likely to be of the same order as that of the forcing inducing it—thousands of kilometers, rather than that of the planetary scale ''conveyor'' circulation. This suggests that the inherent timescale of its variability could be much shorter than that of the global overturning circulation. We will consider a simple model of Ψ_{moc} in section 3 and the appendix.

3. Coupled interactions following ''Bjerknes''

a. The Bjerknes ''compensation'' hypothesis

Bjerknes (1964) discussed the mutual interaction of atmosphere and ocean over the Atlantic in terms of the interplay of meridional heat transport in the two fluids. This is of interest here because it abstracts us away from the details of air–sea interaction. Instead it focuses on, but makes strong assumptions about, the gross heat-transporting properties of the two fluids. He argued that

[3] It is likely that anomalous air–sea heat fluxes at low frequencies are somewhat smaller than plotted in Fig. 3a because air and SSTs equilibrate toward one another on decadal timescales. Moreover, because the Ekman component of anomalous heat flux is likely to vary less with timesscale than the air–sea heat flux, anomalous ocean heat transport may largely balance anomalous Ekman heat transport. For both reasons, the implied ocean heat fluxes plotted in Fig. 3b are likely to be an overestimate of that required to balance air–sea heat flux at low frequencies.

over long timescales changes in heat storage in the ocean could be neglected so that the heat budget for the whole system (atmosphere plus ocean) must be almost completely balanced. If, for example, the net incoming radiation changed in a systematic way over a latitude belt, then the outgoing radiation within that belt would adjust itself to balance—the time-integrated meridional heat fluxes of the joint system could change, but in mutual adjustment to one another so that the sum would remain constant:

$$Q_{\text{atmos}} + Q_{\text{ocean}} = 0, \tag{4}$$

where $Q_{\text{ocean}} = Q_{\text{ig}} + Q_{\text{moc}} + Q_{\text{ek}}$. Thus if Fig. 3b is thought of as an anomalous northward ocean heat transport, then Bjerknes supposed that the anomaly in atmospheric heat transport was exactly opposite—that is, to the south. This, the ''compensation hypothesis,'' is presented schematically in Fig. 6 in terms of the intergyre gyre introduced in section 2.

Suppose, for example, that over a period of time the NAO occupied its high index state more frequently than its low index state. Then, some time later, the intergyre gyre would begin to circulate anticyclonically, $\Psi_{\text{ig}|w} > 0$. This, we imagine, corresponds to the North Atlantic Current having a more pronounced poleward trajectory with an enhanced meridional heat flux, Fig. 6a; $Q_{\text{ig}} > 0$. There will thus be a persistent anomaly in ocean heat flux convergence to the north, raising SST there. Thus to the north of the atmospheric jet stream, whose mean axis is imagined to be coincident with the diagonal of the Z in Fig. 5a, the atmosphere will experience anomalous warming. Anomalous cooling of the atmosphere will be experienced to the south. Note that the curly arrows in Fig. 6 represent *anomalies* in heat flux that are a consequence of ocean dynamics. Anomalous warming to the north and cooling to the south will reduce the meridional temperature gradient across the atmospheric jet stream, which, by thermal wind, will weaken in strength. Thus, one might expect that the poleward heat transport in the atmosphere will fall and so the anomaly in atmospheric meridional heat transport will be to the south, that is, $Q_{\text{atmos}} < 0$, as sketched in Fig. 6 (top). As the atmospheric jet stream weakens, the surface winds and pressure patterns will also weaken, it is supposed, with a slackening of the Icelandic Low. Thus the atmosphere moves to a state in which the NAO(−) phase is preferred [Fig. 6 (bottom)]. In response and over time $\Psi_{\text{ig}|w}$ will change sign to become negative with $Q_{\text{ig}} < 0$, corresponding to the North Atlantic Current taking a more zonal path. This change will be communicated to the atmosphere by air–sea interaction, leading to enhanced atmospheric temperature gradients, $Q_{\text{atmos}} = -Q_{\text{ig}} > 0$, stronger winds, and an increased probability of the NAO occupying its high index state. Hence the cycle can repeat again. The gyre anomaly invoked above is imagined to be a consequence of the state of the NAO blowing over it some time in the past. This delay, which sets the timescale of the oscillation, is a crucial ingredient of models that couple ocean gyres with the atmospheric jet stream (see Latif and Barnet 1994; Jin 1997; Neelin and Weng 1999; Cessi 2000) and is also a central feature of the theoretical model developed here.

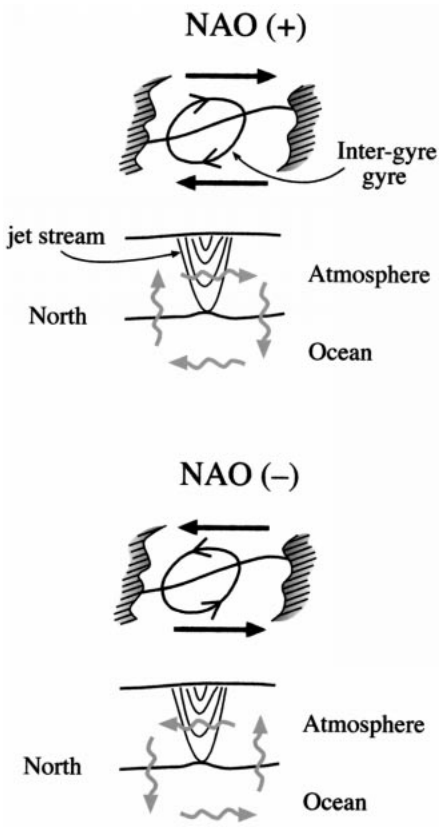

FIG. 6. Schematic of anomalies in air–sea heat flux and atmosphere–ocean heat transport (the curly arrows) that accompany atmosphere–ocean coupling, following Bjerknes (1964). Suppose that for a period of time the NAO occupied its high index state more frequently than its low index state (solid arrows represent surface winds). Then, with some delay, the intergyre gyre begins to circulate anticyclonically, transporting heat poleward. Thus the atmospheric jet stream will experience anomalous warming to the north and cooling to the south. The jet stream will thus weaken, it is supposed, and the anomaly in atmospheric heat transport will be to the south, compensating the enhanced northward oceanic heat transport. With weaker winds, the NAO will occupy its low index state more frequently and so, over time, the sense of the intergyre gyre will change sign to become negative, carrying heat southward. Enhanced atmospheric temperature gradients will result, stronger winds, anomalous poleward atmospheric heat transport, and an increased probability of the NAO occupying its high index state. Hence the cycle, whose period is set by the response time of oceanic heat transport to changes in the atmosphric forcing, can repeat again.

Before going on it should be noted that one might equally well suppose that changes in thermohaline circulation play a role analogous to that of the intergyre gyre. Dipoles in thermal anomalies generated by dipole NAO heat fluxes, can induce anomalous overturning, Ψ_{moc}, as sketched in Fig. 5b, and anomalous heat transport. Thus the curly arrows between the ocean boxes in

Fig. 6 could just as well be thought of as representing anomalous heat transport by thermohaline circulation. Furthermore, if Ψ_{moc} responds to the buildup of meridional gradients in thermal anomalies *with some time delay,* we will see in section 4 that indeed close analogies can be made between the coupling of thermohaline circulation to the overlying jet stream and the coupling of ocean gyres to the jet stream.

The above description of the coupled interaction is highly schematic and makes simple assumptions about the relationship between atmospheric temperature gradients and surface winds, relationships that are much more complicated in nature. For example, the pattern and strength of the climatological surface winds in midlatitudes is primarily controlled through momentum transport by synoptic-scale eddies, which in turn depend on the strength of the zonal wind (see Green 1970). Anomalous momentum transport by synoptic-scale eddies are thought to be the primary excitation mechanism of anomalies such as the NAO, and so they must be invoked in any physical argument that connects SST anomalies to surface wind anomalies. Anomalies in the zonal-mean wind may also be important to the stationary waves. Some of these issues will be discussed below as they arise in the context of the simple coupled model that is now summarized.

b. A simple coupled model

We now attempt to encapsulate the ideas discussed above in a simple model. In an appendix we derive the coupled system from ''first principle'' by integrating the thermodynamic equation for the atmosphere and ocean over elements—boxes—of the Z (Fig. 5) to obtain equations for how the mean temperatures (T_N and T_S) within the respective fluids to the north and south change in response to heat fluxes through the sides of the boxes. We choose the diagonal of the Z to delineate the boxes because we are interested in the modulation of temperature differences *across the mean position of the atmospheric jet stream.* Furthermore there is no mean flow advection of SST anomalies across the diagonal because the mean ocean current flows along it rather then across it. Hence, only *anomalies* in gyre and thermohaline circulation (Ψ_g and Ψ_m) can transport heat laterally between the ocean boxes (see Fig. 7a) and so change the temperatures within the boxes. Temperature differences between the northern and southern ocean boxes modulate air–sea interaction, atmospheric temperature gradients, the strength and latitudinal position of the Atlantic jet stream, and hence the surface wind stress blowing over the ocean. While the thermodynamics is integrated over boxes, the dynamics is not, for we invoke oceanic Rossby waves and thermohaline circulation to set a delay timescale. Because the full derivation is rather lengthy (see appendix) here we only outline the key equations of the coupled model before going on to analyze it in section 4.

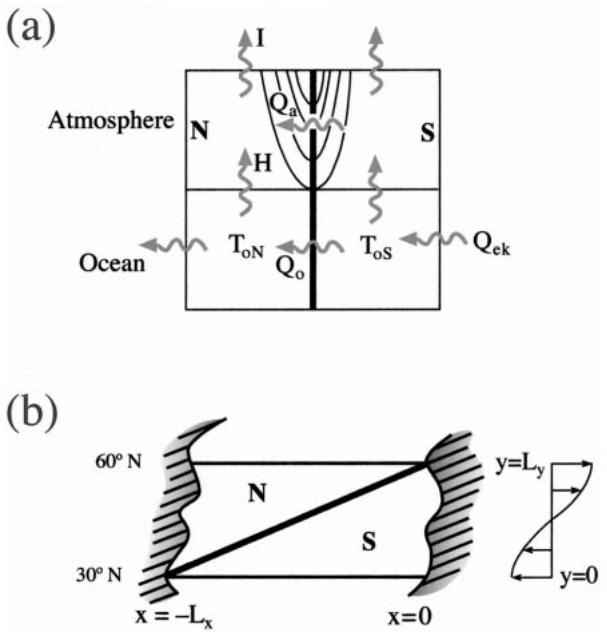

FIG. 7. (a) Vertical section through the ''4-box'' model showing its relation to the Z sketched in Fig. 5a. The thick vertical line corresponds to the position of the axis of the atmospheric jet stream in the climatology, as shown schematically and indicated in the plan view in Fig. 8b. Here N is for north, S for south, and T_o is ocean temperature. The curly arrows are anomalies in heat transport induced by ocean dynamics: Q_o, are ocean heat transport anomalies due to gyres and thermohaline circulation, Q_{ek} are anomalies in Ekman heat transport, Q_a atmospheric heat transport, H are anomalies in air–sea flux and I in longwave radiation to space. (b) Plan view of the Z, and the anomalous winds given by (A20). The eastern boundary is at $x = 0$. The east west scale of the Z is L_x, the width of the Atlantic, the north–south scale is L_y, extending from 30° to 60°N.

The (dimensional) equation for the anomaly in heat content of the upper ocean of depth h in the (for example) northern triangle of the Z is [see Eq. (A10) in the appendix]

$$C_o A \frac{\partial}{\partial t} T_{oN} = Q_M \Psi_m + Q_G \Psi_{g|w} - Q_E \tau - \lambda_{o,a} A (T_o - T_a)_N,$$

where C_o is the heat capacity of the top h meters of ocean, A is the surface area of the northern triangle, and T_{oN} is its temperature anomaly, assumed synonymous with SST. The Q_M, Q_G, and Q_E are scales for heat transport (in PW) due to anomalous thermohaline, gyral, and Ekman circulation across the diagonal of the Z [defined in Eqs. (A11), (A13), (A15)]. The (nondimensional) strength of the anomaly of thermohaline circulation is Ψ_m, Eq. (A12), and $\Psi_{g|w}$ is the (nondimensional) intergyre gyre stream function evaluated just inside the western boundary current [Eq. (A14)]. The (nondimensional) amplitude of the NAO wind stress—sketched in Fig. 7b—is τ, Eq. (A16), and $\lambda_{o,a}$ is the linearized coefficient of combined latent and sensible heat flux representing the damping of SST due to air–sea interaction, defined in Eq. (A9).

Nondimensionalizing T_{oN} with respect to a temperature scale, Υ, and time with respect to t_{delay}, the time it takes a first baroclinic Rossby wave to cross the ocean, the complete coupled system can be written in nondimensional terms thus [Eqs. (A29)–(A32) of the appendix]:

(sea surface temperature)

$$\frac{\partial}{\partial t}T = m\Psi_m + g\Psi_{g|w} - \lambda T + F_T, \tag{5}$$

(gyre)

$$-\frac{\partial}{\partial t}\Psi_g + \frac{\partial}{\partial x}\Psi_g = -\tau, \tag{6}$$

(thermohaline)

$$\frac{\partial}{\partial t}\Psi_m = -sT, \tag{7}$$

(wind stress)

$$\tau = F_\tau - fT. \tag{8}$$

Here g (for gyre) and m (for meridional overturning) [Eqs. (A33) and (A34)] are measures of the efficiency of heat transport by anomalous gyres and thermohaline circulation, respectively; λ [Eq. (A36)] encapsulates the combined effect of air–sea damping and Ekman effects; F_T and F_τ are stochastic forcing terms representing air–sea heat fluxes and wind, respectively; s (for solenoid) [Eq. (A42)] represents the efficiency of thermal dipoles in driving meridional overturning; f (for feedback) [Eq. (A25)] represents the feedback of SST gradients on the NAO wind stress pattern—with $f > 0$, if SST is anomalously cold to the north and warm to the south then we assume a positive NAO is induced, as discussed at length in section c of the appendix.

1) SPECIAL CASES

- Setting $m = g = 0$, Eq. (5) is the archetypal stochastic model of climate variability due to Hasselman (1976) and Frankignoul and Hasselman (1977) in which ocean dynamics plays no role.
- Setting $f = 0$ in Eq. (8), Eq. (6) becomes the stochastic gyre model of Frankignoul et al. (1997), in which there is no coupling between SST and the wind.
- Setting $m = s = 0$ in (5) and (7), our model [Eq. (5) and (6)] has similarities to that studied by Jin (1997), who coupled ocean gyres with the atmospheric jet stream, but with no representation of thermohaline dynamics. There are notable differences between (5) and (6) and Jin's model, however, even when we put $m = s = 0$. Jin (1997) sets $g < 0$ and $f < 0$, assumptions that we find hard to reconcile in the framework of the present model, which invokes an intergyre gyre. It will become clear, however, that the important coupling coefficient is the product $f \times g$ and so if one simultaneously switches the sign of f and g, properties of the coupled system (but not the component parts) remain unchanged. It is difficult to see how g could be negative—an anticyclonic gyre anomaly with $\Psi_{g|w} > 0$ transports heat poleward thus inducing $\partial T/\partial t > 0$, but only if $g > 0$ in (5). The parameter f in (8) could perhaps be negative—although, as discussed in the appendix, models, data, and dynamical considerations suggest that it is positive. We will discuss these issues further as they arise in the analysis of the model in section 4. Neelin and Weng (1999), instead, advect a prescribed climatological temperature with a geostrophic anomaly streamfunction obtained numerically by integration forward of a quasigeostrophic gyre model, in place of the much simpler (5), but with no representation of thermohaline dynamics. They also consider the case where stochastic noise is a function of SST as well as the simple additive processes that is assumed here.
- Setting $g = 0$ in (5), Eqs. (5) and (7) could be viewed as a continuous analog of the stochastic thermohaline box model of Griffies and Tzipermann (1995).

2) NUMERICAL CONSTANTS

Estimates of the various constants and governing nondimensional numbers are given in section d(2) of the appendix but are summarized here.

In Eqs. (5), (6), and (7) time is nondimensionalized with respect to t_{delay}, the time it takes for a first baroclinic mode Rossby wave to cross the ocean. As discussed in the appendix, if we set $t_{\text{delay}} = 1.5 \times 10^8$ s ~ 4 yr, then a period of 8 yr corresponds to a nondimensional frequency of $\omega = \pi$ in these units.

The transport of the intergyre gyre and thermohaline circulation are nondimensionalized with respect to the scales Ψ_G and Ψ_M [see Eqs. (A12)and (A14)] chosen to have values of 10 and 15 Sv, respectively.

The efficiency of heat transport by the thermohaline and gyre circulations, characterized by g and m [defined in Eqs. (A33) and (A44)] and estimated to be (see appendix):

$$g \simeq 10, \tag{9}$$

$$m \simeq 20. \tag{10}$$

One can physically interpret these numbers by inspection of (5): for example, g^{-1} is a measure of the time (in units of t_{delay}) for an intergyre gyre of strength $\Psi_{g|w} = 1$ to change the temperature of the ocean in one of the triangles of the Z by $\Upsilon = 1$ K.

The other timescale of interest is that due to air–sea interaction controlled by the parameter [Eqs. (A36)]. We estimate that

$$\lambda \cong 2.5$$

implying, in dimensional terms, that air–sea interaction will damp a thermal anomaly of 1 K and depth 200 m with an e-folding timescale of $\sim$1.6 yr.

A feedback of SST on wind stress of magnitude

$$f \simeq \frac{1}{5}$$

implies, from (A41), a feedback of SST on wind, $\tau_{\rm SST}$, of magnitude 0.005 N m^{-2} if the SST dipole has magnitude $\sim \pm 1/2$ K and $\tau_{\rm wind}$ in Eq. (A20) is 0.05 N m^{-2}. This is a modest feedback when compared to the magnitude of the NAO(+) wind stress anomaly plotted in Fig. 2a.

Estimates of s are rather problematical and cannot be deduced directly from observations but we judge a typical value to be [see appendix section d(2)]:

$$s \simeq \frac{1}{5}.$$

4. Analysis of coupled model

We now describe the nature of the solutions of (5)–(8). First the uncoupled problem is briefly considered in which the stochastic forcing of the ocean by the wind induces a response in the intergyre gyre that has a red spectrum. We then go on to study the coupled system in which SST anomalies induced by fluctuations in ocean circulation feed back on the winds that drive the ocean. We conclude by an investigation of the role of thermohaline circulation in the coupled problem.

a. Uncoupled

STOCHASTIC FORCING OF GYRES BY WIND

Setting $f = s = 0$ we obtain the gyre model studied by Frankignoul et al. (1997) in which stochastic forcing by the wind induces decadal variability in the ocean. The mathematical form of the solution with $f = s = 0$ is a limit case of the coupled problem studied next, and so we will postpone discussion of those details. Here we note that if the standard deviation of the stochastic wind stress forcing is 0.05 N m^{-2}, roughly consistent with the observations, then $\Psi_{g|w}$ reaches $\pm 1/3$ or so (± 3 Sv in dimensional units)—see Fig. 8a. As the gyre fluctuates in strength, so does its meridional heat transport (see axis on rhs of Fig. 8a) inducing, from (5), changes in temperature, T. The magnitude of the temperature changes depend on the efficiency of the air–sea damping processes, controlled by the parameter λ. If $\Psi_{g|w} \sim 1/3$, then $g\Psi_{g|w} \sim 3$ and balancing with λT yields a temperature anomaly of about 1 degree if $\lambda = 3$. Moreover, because Q_g depends on $\Psi_{g|w}$, these temperature changes induced by ocean dynamics, will have decadal timescales. Thus the observed level of stochastic atmospheric forcing is sufficient to induce changes in the intergyre gyre that contribute importantly to SST variability provided that λ is not too large—spectra of western boundary current transport are presented in Frankignoul et al. (1997); Jin (1997) and Neelin and Weng (1999) also present spectra of associated SST variability, with and without coupling.

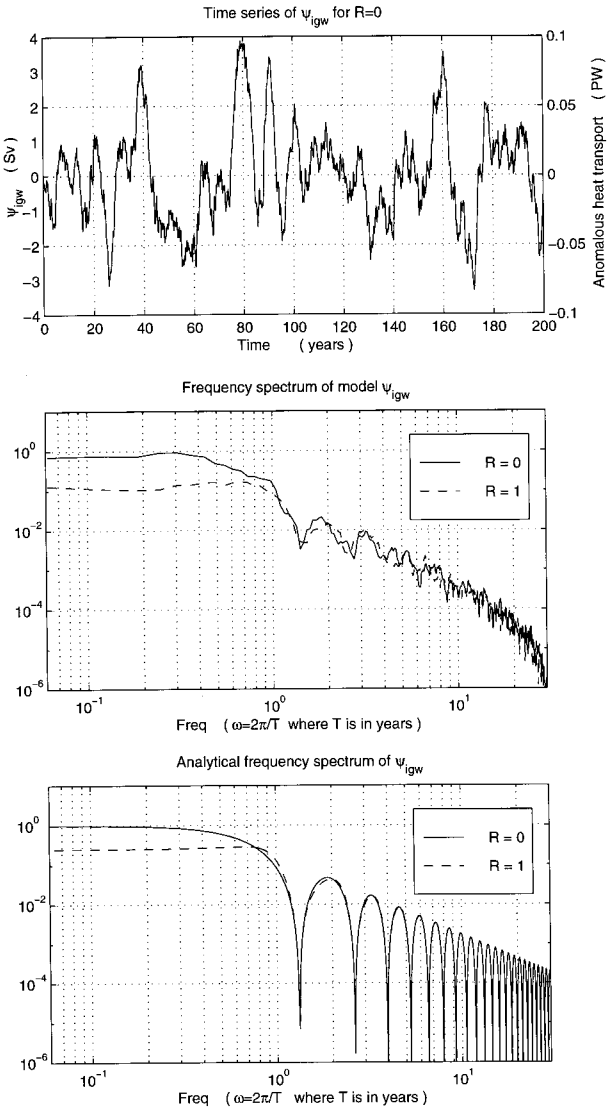

FIG. 8. (a) Time series of volume transport (Sv, left axis) and heat transport (PW) of the intergyre gyre (right axis) obtained by integration of (12) with white noise forcing and $R = 0$. (b) Power spectrum of stochastically forced intergyre model computed from numerical time series with $R = 0$, 1 and (c) predicted analytically from (15). In (b) and (c), $\omega = 1$ corresponds to a period of 2π years.

Let us now consider the feedback on ocean circulation of the winds that are forced by these SST anomalies.

b. Coupled

1) THE BJERKNES COMPENSATION LIMIT

We set s and thus Ψ_m to zero, so enabling gyre dynamics to be studied in isolation, and consider the limit discussed by Bjerknes (1964) in which heat storage is neglected. If $\partial T/\partial t = 0$ in (5), then atmospheric heat

transport anomalies exactly balance oceanic heat transport anomalies and

$$\lambda T = g\Psi_{g|w} \tag{11}$$

neglecting stochastic thermal forcing terms. Thus (6) becomes, using (8),

$$-\frac{\partial}{\partial t}\Psi_g + \frac{\partial}{\partial x}\Psi_g = R\Psi_{g|w} + F_\tau, \tag{12}$$

where the coupling constant R is

$$R = \frac{fg}{\lambda} \tag{13}$$

and F_τ is the imposed mechanical forcing of the gyre. Following Frankignoul et al. (1997), we assume F_τ to be a stationary random process with zero mean and a spectrum that is white in frequency space:

$$F_\tau = \hat{F}e^{i\omega t}, \tag{14}$$

where ω is the frequency of the imposed forcing and $\hat{F}$ is constant.

To satisfy the differential Eq. (12) and the condition that $\Psi_g = 0$ at the eastern boundary, $x = 0$, then Ψ_g must vary in x like $(1 - e^{ikx})$ with ω and k related thus:

$$\frac{\omega}{k} = 1,$$

where k is the zonal wavenumber and the zonal phase speed is $c = -\omega/k = -1$. Noting that $\Psi_{g|w}$ is evaluated at $x = -1$, we find that:

$$\Psi_g = \frac{(e^{ikx} - 1)e^{i\omega t}}{\left[1 + \dfrac{R}{i\omega}(1 - e^{-ik})\right]}\frac{\hat{F}}{i\omega}. \tag{15}$$

Setting $R = 0$, we obtain the solution of Frankignoul et al. (1997). If $R \neq 0$, then power in frequencies $\omega < R$, are damped relative to the Frankignoul et al. reference—see Figs. 8b and 8c where power spectra of $\Psi_{g|w}$ [and hence, in view of (11), T also] are plotted. This damping arises because the heat carried by the ocean at low frequencies induces temperature anomalies in the ocean, which feed back on atmospheric winds in such a sense that they always oppose the preexisting sense of circulation of the intergyre gyre, thus reducing its power at these frequencies: it is the state of affairs skectched in Fig. 6. This will be an important feature of the coupled model even when heat storage is taken into account because the limit of vanishing $\partial T/\partial t$ is appropriate at very low frequencies.

Studies of the free modes of the system—$F_\tau = 0$ in (12)—whose dispersion relation is obtained by setting the denominator in Eq. (15) to zero—shows that there are only decaying oscillatory modes, as one would intuitively expect by inspection of (12). In the limit that R becomes large, however—strong feedback of SST on wind (f large) and/or weak damping (λ small)—then the oscillations decay very slowly. Note, however, that in the region of parameter space relevant to the ocean—$fg \sim \lambda \sim 3$ [see section 4b(2)]—we find that $R \sim 1$ and the above model predicts strong damping with the Rossby wave signal decaying toward zero before it has had chance to cross the basin. Moreover, at the timescale of interest ($\omega \sim 3$), then the neglect of the $\partial T/\partial t$ term in (5) cannot be justified—the compensation limit of Bjerknes, (11), is compromised because of heat storage. We therefore move on to consider the fuller problem.

2) Interpretation as a delayed oscillator

To proceed further, and with a minimum of algebraic complexity, we study the free modes of the coupled system retaining $\partial T/\partial t$ in Eq. (5), but phrasing the problem explicitly as a delayed oscillator model. From Eq. (6) we can write, setting $F_\tau = 0$:

$$\Psi_{g|w} = -f\int_{t-1}^{t} T\,dt \simeq -fT\left(t - \frac{1}{2}\right), \tag{16}$$

expressing the fact that, in the absence of external stochastic forcing, the anomaly in western boundary current transport depends on the wind induced by temperature anomalies, τ_{SST}, acting on the ocean over the previous Rossby wave transit time. Then our coupled system can be written:

$$\frac{\partial}{\partial t}T = m\Psi_m - fgT\left(t - \frac{1}{2}\right) - \lambda T,$$

$$\frac{\partial}{\partial t}\Psi_m = -sT, \tag{17}$$

explicitly revealing the role of Rossby wave propagation as a delay mechanism (see Jin 1997). A more complete and involved analysis of the system, (5) and (6), but with $m = s = 0$, is presented in Jin (1997), who does not make the approximation Eq. (16). Note that although he assumes $f, g < 0$, the product $f \times g > 0$, as here. It can be shown that the leading modes and marginal stability conditions of the full equations are reproduced well when the approximate form (17) is used and $fg > 0$. Equation (17) also explicitly draws out the essential nature of the problem and the possibility of oscillatory behavior: there is a negative feedback (λT), the possibility of a positive feedback (the terms in fg and m), and a delayed adjustment process between the two (Suarez and Schopf 1988; Battisti and Hirst 1989). Before going on it should be remembered that, because of Ekman layers, λ in (17) also depends on f [see (A36)].

Looking for solutions of the form T; $\Psi_m \sim e^{\sigma t}$, we obtain the following dispersion relation

$$\sigma^2 + \tilde{\lambda}\sigma + sm = 0, \tag{18}$$

where

$$\tilde{\lambda} = \lambda + f\tilde{g}, \qquad \tilde{g} = ge^{-(1/2)\sigma}.$$

Writing

$$\sigma = \sigma_r + i\sigma_i$$

substituting into (18), and equating real and imaginary parts, we obtain

$$\sigma_r^2 - \sigma_i^2 + \tilde{\lambda}_r\sigma_r - \tilde{\lambda}_i\sigma_i + sm = 0,$$
$$2\sigma_r\sigma_i + \tilde{\lambda}_r\sigma_i + \tilde{\lambda}_i\sigma_r = 0, \qquad (19)$$

where

$$\tilde{\lambda}_r = \lambda + fge^{-(1/2)\sigma_r}\cos\frac{\sigma_i}{2},$$

$$\tilde{\lambda}_i = -fge^{-(1/2)\sigma_r}\sin\frac{\sigma_i}{2}.$$

Let us consider some special cases.

(i) No thermohaline circulation; s = 0.

The dispersion relation (18) reduces to

$$\sigma = -fge^{-(1/2)\sigma} - \lambda, \qquad (20)$$

which is of the same form as the archetypal delayed oscillator model for ENSO [see Battisti and Hirst (1989), their Eq. (2.10)]. Here, however, the interpretation of the terms is somewhat different. In the midlatitudes problem observations strongly suggest that λ (which represents the sum of all those processes that induce *local* changes in SST) is positive and so local processes induce decay. In the tropical eastern Pacific, however, anomalous upwelling can, perhaps, lead to λ becoming negative and so local processes may themselves lead to growth.

Multiplying (20) by its complex conjugate we obtain

$$(\sigma_r + \lambda)^2 + \sigma_i^2 = (fg)^2e^{-(1/2)\sigma_r}.$$

For small growth rates ($\sigma_r \ll \lambda$), and when air–sea interaction dominates ($fg \ll \lambda$) only decaying, nonoscillatory solutions are possible. But for small growth rates ($\sigma_r \ll \lambda$) and if local processes do not dominate ($fg > \lambda$), then oscillatory solutions are possible. Note, however, that the physically relevant region of parameter space is $fg \sim \lambda \sim 3$.

Marginal stability of the delayed oscillator model ($\sigma_r = 0$) occurs when

$$\sigma_i - fg\sin\frac{\sigma_i}{2} = 0, \qquad (21)$$

$$\lambda + fg\cos\frac{\sigma_i}{2} = 0. \qquad (22)$$

Figure 9a plots the frequency of the mode, σ_i, at neutral stability, at which point $\sigma_i^2 = (fg)^2 - \lambda^2$, and the critical coupling coefficient, fg, as a function of λ. Jin (1997) also considers the case in which $\lambda < 0$, noting the connection to the theory of ENSO modes. But here, in middle latitudes, λ is unlikely to be negative. We see that:

1) If $\lambda = 0$ (no damping) then $fg > \sigma_i = \pi$ for unstable modes to be allowed. If $\lambda > 0$, the critical value of fg must be larger than π but, in the limit of large λ, $fg/\lambda \to 1$ at marginal stability. The central role of the parameter $R = fg/\lambda$, the coupling constant in (12), is again clear, as could have been anticipated by inspection of Eq. (17).
2) The frequency of the neutral mode lies in a narrow range, between $\pi < \sigma_i < 3\pi/2$, over a wide range of λ, corresponding to a period between 4/3 and twice the Rossby wave propagation period.

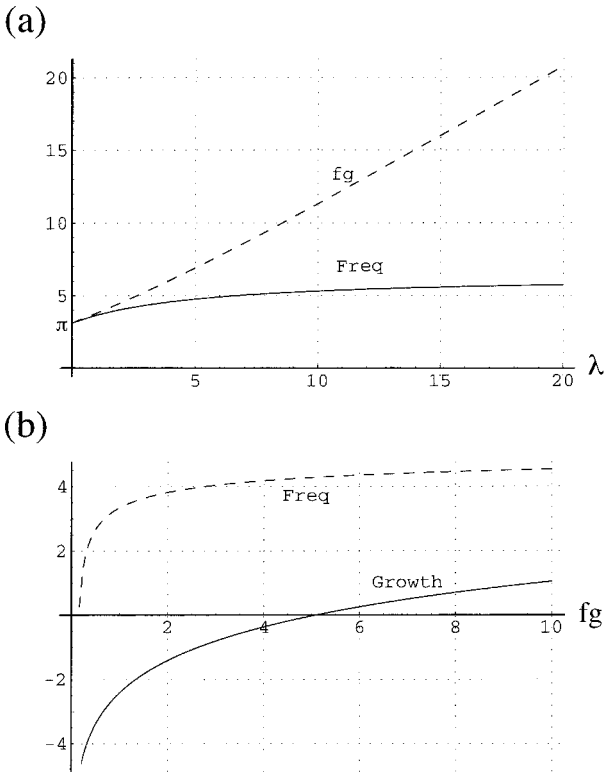

FIG. 9. (a) The frequency σ_i and fg at neutral stability plotted against λ obtained by solving (21) and (22) (b) growth rate σ_r and frequency σ_i plotted as a function of fg for $sm = 0$ and $\lambda = 2.75$. obtained by solving (19).

When $\lambda \sim 2$, inspecting Fig. 9a we find that at neutral stability $fg \sim 4$ which, using (A36), tells us that $f \sim 0.4$ if $g \sim 10$.

In Fig. 10 the same information is presented in dimensional form and perhaps in a more physically appealing way—the critical value of $f(Q_G/AY)$ required to achieve marginal stability is plotted against $(C_o/t_{\text{delay}})\lambda$, where from (A36), (A37), and (A39),

$$\frac{C_o}{t_{\text{delay}}}\lambda = \lambda_o - f\frac{H_{ek}}{Y}.$$

Note that both axes are now in units of watts per square

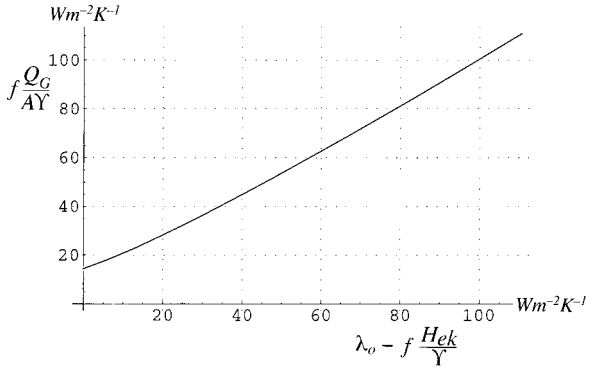

FIG. 10. The quantity $fQ_G/A\Upsilon$ as a function of $\lambda_o - fH_{ek}/\Upsilon$ at marginal stability for $sm = 0$.

meter per Kelvin, the unit of the damping coefficient λ_o, and that $(fQ_G/A\Upsilon)/(\lambda_o - fH_{ek}/\Upsilon)$ is just R, Eq. (13) written out in detail. Frankignoul et al. (1998) show convincingly, by analyzing the covariance between observed winter–time SSTs and observed fluxes, that $\lambda_o \sim 20$ W m^{-2} K^{-1} in the North Atlantic. If f were equal to unity, then Fig. 4b shows that the magnitude of the Ekman term in the above is significant since it is of the correct sign to partially offset damping by air–sea interaction, which cools to the north and warms to the south in the positive phase of the NAO. If $f \approx 0.4$, as estimated above, then Ekman processes are still seen to provide a positive feedback on SST, particularly in the regions of strongest SST anomalies (compare Fig. 4b to Fig. 2b), just where they are most effective. The physically relevant section of the abscissa of Fig. 10, then, is in the range 10–20 W m^{-2} K^{-1} and so $fQ_G/A\Upsilon$ must be in the range 20–30 W m^{-2} K^{-1} to achieve marginal stability and oscillatory behavior. Is this possible or likely?

It is first worth reminding ourselves that, in the framework of our simple model, fQ_G is the heat delivered by the intergyre gyre to the northern ''triangle'' of the Z, associated with its driving by winds induced by SST anomalies. In the appendix we estimate Q_G to be $\sim 1/4$ PW and $A = 4.5 \times 10^{12}$ m^2—thus $Q_G/A\Upsilon \sim 50$ W m^{-2} K^{-1}. Thus f, the feedback of SST on wind, must be in the range 0.4–0.6 to reach marginal stability. This—see (A41)—is a stress of 0.0125 N m^{-2} if $T_{oN} = 1/2$ K and should be compared to the unit strength of the NAO stress anomaly, $\tau_{\text{wind}} = 0.05$ N m^{-2} (as suggested by Fig. 2a). If the stress is related to the wind by $\tau = \rho_a c_D u_s^2$, where u_s is the surface wind, then $\tau_{\text{SST}}/\tau_{\text{wind}} \sim 2u_s'/\overline{u_s}$. Thus we require a surface wind anomaly of strength $u_s'/\overline{u_s} \sim 0.0125/(2 \times 0.05) \sim 0.125$, which is only ~ 0.6 m s^{-1} if $\overline{u_s} = 5$ m s^{-1}. This is equivalent to a pressure change of less than 1 mb in 1000 km in response to the dipole SST anomaly of $\pm 1/2$ K.

Modeling results (Rodwell et al. 1999) suggest that an atmospheric response to SST anomalies of order 1 m s^{-1} per 1° SST anomaly are not unreasonable. The analysis of the surface stress response of ECHAM 2 to SST anomalies in the Atlantic presented in Fig. 2 of Neelin and Weng (1999) suggests that f can indeed reach ~ 0.4 giving $fg \sim 4$ if $g = 10$. Figure 9b plots the growth rates predicted by the delayed oscillator model, as a function of fg. We observe weakly damped/growing modes in the range $4 < fg < 6$, which could be readily excited in the presence of stochastic noise.

(ii) Including thermohaline circulation; $s \neq 0$.

In the absence of ocean gyres, $fg = 0$, we obtain damped oscillations with

$$\sigma_i^2 = sm - \frac{\lambda^2}{4}, \qquad \sigma_r = -\frac{\lambda}{2}.$$

The natural frequency $\sqrt{sm}$ can be excited by stochastic atmospheric forcing, provided the damping is sufficiently weak. If the damping is strong, however, such that $\lambda^2/4 > sm$, then we obtain pure damping with no oscillations at all; ''critical damping'' occurs when $\lambda^2/4 = sm$ in which case the system when perturbed by external forcing smoothly moves to its new equilibrium without oscillation or overshoot. If $s = 1/5$, $m = 20$, and $fg = 0$, then $sm = 4$ and $\lambda^2/4 \sim 2.5$ suggesting that oscillations will be damped rather rapidly by air–sea interaction.

When $fg \neq 0$, marginal stability occurs when, setting $\sigma_r = 0$ in (19):

$$\sigma_i\left(\sigma_i - fg \sin\frac{\sigma_i}{2}\right) = sm, \tag{23}$$

in place of (21) with (22) remaining the same.

Figure 11 plots the critical coupling coefficient, fg, and the frequency of the mode, σ_i, at neutral stability, as a function of λ for different values of thermohaline coupling sm. Note that for $sm = 0$ we obtain the curves shown in Fig. 9. We see that as sm is increased, the frequency of the mode *increases* and the value of the critical coupling coefficient *decreases*. In particular, at $\lambda = 0$ then $\sigma_i = \pi$ and

$$fg > \pi - \frac{sm}{\pi}$$

for growing modes. If $s = 1/5$ and $m = 20$ then fg must exceed only 1.9 rather than π if $s = 0$. This brings f down to only 0.2 if $g = 10$.

Thus we see that if thermohaline variability is governed by an equation of the form (7), then it can play a catalytic role, making it easier for the delay introduced by the gyre to destabilize the system.

c. The role of thermohaline circulation

We saw above that, for the particular model of thermohaline dynamics assumed, its inclusion did not fundamentally alter the nature of the coupled problem, although the conditions for marginal stability were mod-

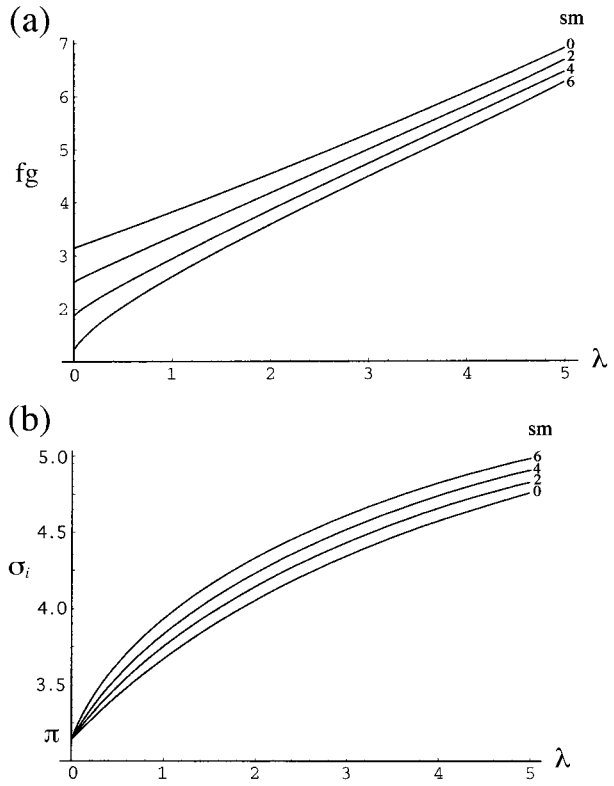

FIG. 11. The quantities (a) fg and (b) σ_i at neutral stability plotted against λ for different values of thermohaline coupling sm, obtained by solving (22) and (23).

ified and, in fact, made rather easier to achieve. In the absence of gyre dynamics our model of thermohaline circulation, (7), leads to damped harmonic oscillation, when coupled to (5). The essential reason is that Eq. (7) does not introduce a delay in to (17).

A commonly held view is that the thermohaline circulation rather quickly comes into balance with changing boundary conditions and forcing, on a timescale set essentially by the propagation speed of Kelvin waves (Kawase 1987). Kawase investigated the response of a shallow water model to mass injection at the northwestern boundary and studied the emanation of Kelvin waves along the boundary and across the equator. Assuming a mean gravity current of 2 m s^{-1}, one obtains a travel time down the western boundary of only a few months. If the adjustment time of the thermohaline circulation is indeed this rapid, it is appropriate to set $\partial/\partial t$ to zero in (7) and balance the solenoid term by a frictional term, in ε, thus:

$$\varepsilon\Psi_m = -sT. \tag{24}$$

If this is the equation governing thermohaline dynamics, it merely introduces another damping process into (17).

Marotzke and Klinger (2000), however, in a study of the spinup of the thermohaline circulation using the Geophysical Fluid Dynamics Laboratory (GFDL) numerical model, strongly argue against such a rapid adjustment timescale. They show that density anomalies induced in the north by convection are *advected* southward by the deep western boundary current. It is the advective timescale of the western boundary current, from years to decades, that controls the adjustment timescale of the overturning to changes in forcing. This advective timescale introduces a delay. Joyce et al. (2000) review observational evidence, and develop a simple conceptual model, of the delay between the transport of Labrador Sea Water at the Gulf Stream separation point and its creation by convection in the Labrador Sea.

Let us suppose, then, that in analogy with (16),[4]

$$\Psi_m = -s\int_{t-1}^{t} T\,dt \simeq -sT\left(t-\frac{1}{2}\right), \tag{25}$$

but now we imagine the delay mechanism to be advection of convectively modified waters—for example, modified by the northern half of the dipole forcing that pushes in to the Labrador Sea in Fig. 3a. Equation (25) looks back in time over that delay period, and so the strength of the thermohaline circulation at any time depends on the integral of the dipole solenoid term forcing over that period. The delay time will, of course, generally be different from that of first baroclinic Rossby waves propagating across the ocean basin, but for the sake of simplicity we have supposed that $t_{\text{delay}|\text{moc}} = t_{\text{delay}|\text{gyre}}$. There are interesting interactions between Ψ_m and Ψ_g, particularly when $t_{\text{delay}|\text{moc}} \neq t_{\text{delay}|\text{gyre}}$, but we will not consider them here.

1) COUPLING WITH MOC IN THE ABSENCE OF GYRES

If (25) is our model of the response of thermohaline circulation to forcing, rather than (24) or (7), then in the absence of ocean gyres ($g = 0$) the analysis of section 4b(2) carries over unchanged on replacing f with s and g by m. The conditions for marginal stability are given by (21) and (22) with $fg \to sm$. Thus Fig. 10 is also appropriate for the coupling of thermohaline circulation with an atmospheric jet stream if we interpret the ordinate as $sQ_M/A\Upsilon$. Thus again $sQ_M/A\Upsilon$ must be in the range 20–30 W m^{-2} K^{-1} to achieve marginal stability. Setting Q_M to 1/2 PW and using the same value of A, then s must exceed 1/3. If $T = 1/2$, then $\Psi_m = \Psi_{\text{mac}}/\Psi_M \sim 1/6$, implying a thermohaline circulation anomaly of ± 2.5 Sv, if $\Psi_M = 15$ Sv, roughly as has been observed in models and in accord with inferences from observations.

[4] The differential equation that goes along with the integral equation (25) is $\partial\Psi_m/\partial t - |\overline{V}|\partial\Psi_m/\partial y = -sT$, where $|\overline{V}|$ is the southward meridional advective speed associated with the mean MOC at which the anomaly is advected. The close analogy with (6) and (8) is evident.

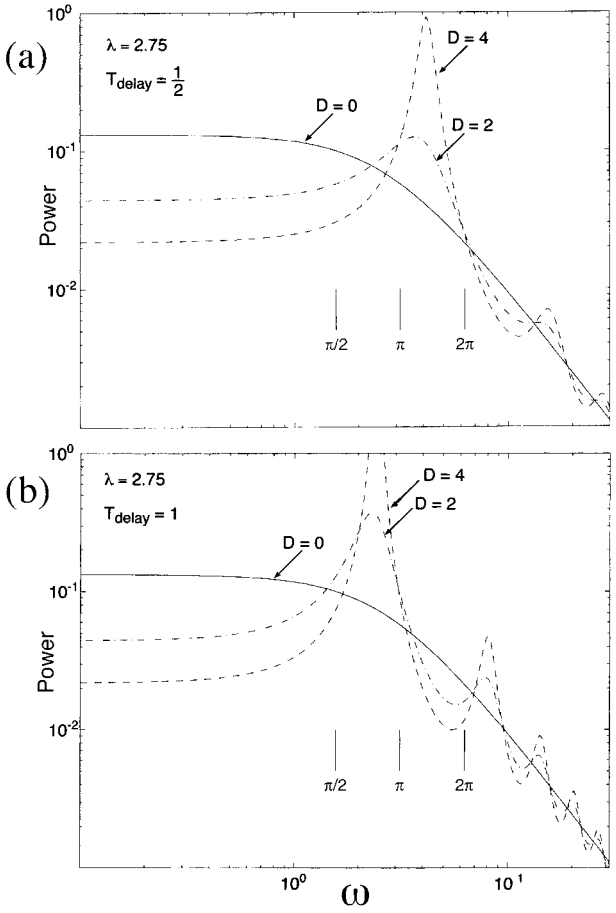

FIG. 12. Power spectrum of stochastically forced delay model computed from Eq. (27) with $\lambda = 2.75$ as a function of D for two delay times (a) $t_{\text{delay}} = 1/2$ and (b) $t_{\text{delay}} = 1$. The period corresponding to $\omega = \pi$ is, dimensionally, ~12 yr, if $t_{\text{delay}} = 4$ yr.

2) STOCHASTICALLY FORCED THERMOHALINE MODEL

Now we have

$$\frac{\partial}{\partial t}T = -DT(t - t_d) - \lambda T + F_T, \tag{26}$$

where D (for delay with time t_d) is $D = sm$, the delay term due to thermohaline circulation and F_T is a stochastic forcing term. For a component $F_T = \hat{F}_T e^{i\omega t}$, (26) has solutions:

$$\hat{T} = \frac{\hat{F}_T}{(i\omega + De^{-i\omega t_d} + \lambda)}. \tag{27}$$

The power spectrum is plotted in Fig. 12 for various values of D at two different delay times: $t_d = 1/2$ and 1 in (26). When $D = 0$ we observe the canonical behavior: a red spectrum at high frequencies that levels out when $\omega \lesssim \lambda$. But when $D \neq 0$, we observe a peak at the natural frequency of the system corresponding to, in the case $t_d = 1/2$, $\omega \sim \sigma_i \sim 4.5$ (see Fig. 11b when $\lambda \sim 2.75$). Note that the natural modes of the system are weakly damped in the case $D = 2 \lesssim \lambda = 2.75$. The peak becomes more marked as D increases through its critical value and is unrealistically large for $D = 4$. If the delay timescale is longer, the peak shifts toward lower frequencies. The spectral peaks seen in Fig. 12 are notably absent in Fig. 8, due to the neglect of heat storage in the latter.

5. Discussion and conclusions

Air–sea interaction in midlatitudes leads to strong damping of SST and associated oceanic thermal anomalies at a rate controlled by λ if local processes dominate, as in the Hasselman (1976) canonical model of climate variability, written here in our nondimensional form:

$$\frac{\partial T}{\partial t} = -\lambda T + F_T.$$

In middle latitudes there do not appear to be *local* processes analogous to equatorial upwelling events associated with ENSO that can significantly offset this strong local damping. As long as local processes dominate, air–sea interaction will rapidly damp the characteristic patterns of SST anomaly induced by stochastic NAO forcing.

Here we have discussed, motivated by inspection of the patterns of NAO stresses and air–sea fluxes in section 2, how changes in ocean gyres and thermohaline circulation induced by NAO forcing (essentially meridional shifts in the atmospheric jet stream) could lead to anomalous advection of heat, which modify, and perhaps fundamentally change, the nature of the above balance in the vicinity of the separated Gulf Stream on interannual-to-decadal timescales. These nonlocal processes can turn the above into ''delayed oscillator'' form (26), in which the delay term can be due to gyre dynamics ($D = fg$) or thermohaline circulation ($D = sm$), or terms representing a combination of the two, with obvious connections to the theories of ENSO outlined in, for example, Battisti and Hirst (1989). Moreover, as shown in section 4, the form (26) arises naturally out of thermodynamical and dynamical considerations motivated by observations reviewed in section 2, making the physical interpretation of the terms and nondimensional numbers rather transparent.

Following Battisti and Hirst (1989) insight into the role of ocean circulation in (26) can be obtained by multiplying it through by T to yield (setting $F_T = 0$):

$$\frac{1}{2}\frac{\partial T^2}{\partial t} = -DTT\left(t - \frac{1}{2}\right) - \lambda T^2.$$

Whether T^2 grows or decays from one maximum to the next depends on the sign of $D \int TT(t - 1/2)\, dt$ relative to $\lambda \int TT\, dt$ over the period of the oscillation. If there is a negative correlation between T and $T(t - 1/2)$ over the period, then growth is possible. This can occur when

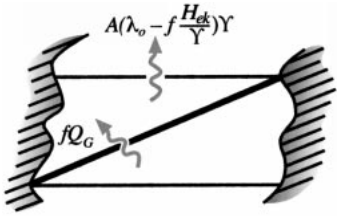

FIG. 13. Schematic diagram showing the role of ocean circulation in the coupled problem. The controlling parameter is $R = fQ_G/[A(\lambda_o - fH_{ek}/\Upsilon)\Upsilon]$. The numerator is the heat carried across the diagonal of the Z by ocean currents driven by SST-induced wind anomaly. The denominator is the heat lost due to damping of SST anomalies in the triangle to the north, less the feedback due to Ekman processes. If $R \sim 1$, weakly damped/growing oscillatory solutions are possible, because then advection of heat by anomalous currents can balance locl damping of SST anomalies by air–sea interaction.

the period of the oscillation in T is between, roughly, 1 and 2 delay times and D is sufficiently large. Studies of the stability of the coupled system in section 4 indeed show that ocean circulation, if delayed, can offset the effect of damping, bringing the coupled system to neutrality, weak damping or even growth, provided that $R = D/\lambda$ is sufficiently large. If R exceeds a critical value [that $R \gtrsim 1$ as suggested intuitively by inspection of (26)], then stochastic forcing by NAO variability can ''ring'' the system exciting oscillatory modes rather than be resisted by strong damping. Note that it is not of much practical import whether *unstable* modes exist, only that $R \gtrsim 1$—in middle latitudes there is a wealth of stochastic variability to energize neutral or weakly damped modes.

This critical condition on $R = fQ_G/[A(\lambda_o - fH_{ck}/\Upsilon)\Upsilon]$ can be understood with reference to the schematic diagram (Fig. 13). Consider for a moment the role of the intergyre gyre. The numerator of R is just the heat carried across the diagonal of the Z by anomalous currents driven by SST-induced wind anomaly. The denominator is the heat lost due to damping of SST anomalies in the triangle to the north, less the feedback due to Ekman layers. If the nonlocal process, advection by the gyre, balances the local one, damping by air–sea interaction, then neutrality is achieved and stochastic forcing will excite oscillations in the coupled system with a timescale set by the delay in the gyre response. Note that the numerator depends on both f, the feedback of SST on the NAO, *and* the efficiency of the intergyre gyre heat transport mechanism Q_G. Even though f may be small, fQ_G can be significant if Q_G is large. In the Atlantic Ocean Q_G may indeed be large because it is associated with subtle changes in the Gulf Stream/North Atlantic Current system, which, in the mean, carry huge quantities of heat meridionally and are sensitive to meridional shifts in the surface stress pattern. Our interpretation and association of Q_G with an intergyre gyre is important in this regard: the meridional shift of the zero-curl line is a central ingredient of the mechanism because shifts, in contrast to changes in wind curl amplitude, can induce large anomalous heat transport across the climatological boundary of the gyres. We estimated in section 4 that f must reach about 1/2 to achieve neutral stability, which corresponds to a τ_{SST} of 0.0125 N m^{-2} if $T_{oN} = 1/2$ K, much as is observed in atmospheric models driven by midlatitude SST anomalies. A τ_{SST} of this magnitude can, from (A22), drive an intergyre gyre of magnitude $\Psi_{ig|w} \sim \pm 2.5$ Sv with a heat transport of $\sim \pm 0.07$ PW if $Q_G = 1/4$ PW, sufficient to balance air–sea interaction and suggesting that the delay term in (26) may indeed play a role. The denominator of R also depends on f: the positive feedback of Ekman layers on SST acts to partially offset damping of SST due to air–sea interaction, increasing R and helping to bring the system toward neutrality.

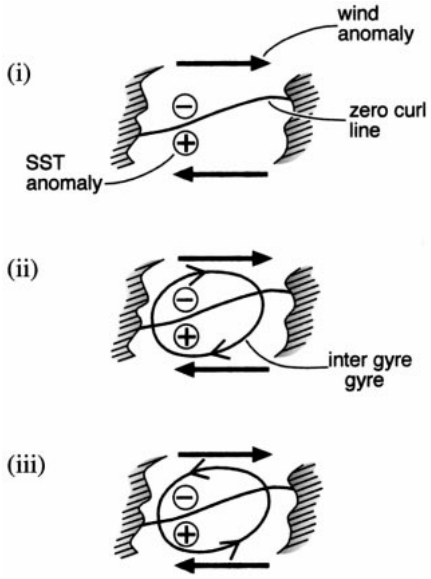

FIG. 14. The phase of the intergyre gyre, SST, and the anomalous winds as a function of frequency according to our delayed oscillator gyre model. On short time scales, (i) SST passively responds to NAO forcing generating low SST to the north and warm SST to the south. On very long timescales, (ii) ocean circulation damps SST anomalies, reducing the power in its spectrum at low frequencies relative to the case of no ocean circulation—see Fig. 12. At resonant frequencies, (iii) ocean circulation enhances SST anomalies.

Figure 14 shows the phase of the intergyre gyre, SST, and the anomalous winds in the high NAO state as a function of frequency according to our delayed oscillator gyre model. On short timescales, (i) SST passively responds to NAO forcing generating anomalously low SST to the north and warm SST to the south. On very long timescales, (ii) the Bjerknes limit sketched in Fig. 6, ocean circulation damps SST anomalies, reducing the power in its spectrum at low frequencies relative to the case of no ocean circulation (see Fig. 12). At resonant frequencies, (iii) ocean circulation enhances the power in SST anomalies relative to the canonical model.

In the case of thermohaline circulation, $fQ_G \rightarrow sQ_M$ and similar arguments apply if thermohaline circulation introduces a delay, but the dynamics we have assumed

for time-dependent thermohaline circulation are sufficiently tentative that its role requires further elucidation. We believe that thermohaline circulation can indeed introduce important delay timescales and, moreover, timescales that could be as short as that associated with gyre dynamics. The dipole of NAO forcing does not ''pull'' the whole planetary-scale conveyor but rather introduces anomalies in overturning circulation that are local to it and so may be associated with rather short (less than about decadal) timescales. The role of thermohaline circulation is probably best studied by designing numerical experiments that focus on the mechanism of time-dependent thermohaline circulation in response to stochastic dipole forcing.

The mechanism described here—with its emphasis on an intergyre circulation anomaly driven by and inducing meridional shifts in the zonal wind pattern—provides a simplified framework to explore the ideas first set out by Bjerknes (1964). In a broad sense it also has much in common with the gyre-jet mechanism of Latif and Barnett (1994), although many of the details differ. In its focus on SST dipole anomalies in the vicinity of the separated Gulf Stream, it addresses the genesis mechanism of SST anomalies that are observed to progress westward in observations by Sutton and Allen (1997) and Hansen and Besdek (1996), and in models by Visbeck et al. (1998). The perspective given by the intergyre gyre mechanism is one of a strongly damped standing wave oscillator, energized by basinwide stochastic forcing. It emphasizes the standing-wave aspects of the problem, but superimposed on it will be the slow advection of anomalies by the mean currents, as suggested by the observations of Sutton and Allen (1997).

No attempt has been made here to incorporate the seasonal cycle into our model. There are two important issues. In our scale estimates we have chosen strengths typical of the wintertime NAO; although the NAO has significant power in the summer months and a nonnegligible amplitude during the whole year, the annual mean forcing is a factor (<1 and ~ 0.6; A. Czaja 2000, personal communication) of the wintertime NAO. Second, the wintertime NAO will be associated with wintertime SSTs, which are in contact with deep thermal anomalies that become capped in the summertime and reemerge the following winter. This capping is likely to reduce the effective damping of SST anomalies; thus the annual mean air–sea damping, λ, is perhaps also a factor (<1) of the wintertime value assumed here. Thus these two aspects are likely to offset one another in terms of their effect on the critical parameter R, one appearing on the denominator, the other in the numerator.

We have made gross assumptions about the effect of SST anomalies on the surface stress field beneath the atmospheric jetstream—as expressed in (8). Experiments with AGCMs suggest that midlatitude SST anomalies have a rather small influence on the atmospheric jet stream. However, the all-important meridional shifts in the surface patterns are subtle and even though they may not be large, they can be associated with very significant air–sea flux anomalies. Further experiments with AGCMs, perhaps driven by surface flux anomalies rather than SST, are required with the ideas set out here in mind.

Last, the mechanisms discussed in this paper have characteristic spectral signatures in SST and sea level pressure that are being sought in the observations and will be reported later.

Acknowledgments. Discussions with Paola Cessi and Arnaud Czaja at various stages in the development of this study were much appreciated. We should like to acknowledge the NOAA Office of Global Programs, whose support made this work possible. Helen Johnson was supported by the Physical Oceanography program of NSF during her stay at MIT. The observational data presented in section 2 was kindly made available to us by Martin Visbeck of Lamont.

APPENDIX

Derivation of Coupled Model

a. Heat budget of the upper ocean

Consider the 4-box model sketched in Fig. 7. The boxes can be considered to represent regions on either side of the climatological position of the zero-wind-stress-curl line in the North Atlantic, the diagonal of the Z in Fig. 5a. There are two boxes in the atmosphere and two in the ocean. The atmospheric boxes extend over the depth of the troposphere: the ocean boxes are imagined to be deep enough to contain within them the fluid that undergoes modification by air–sea interaction. We imagine that stochastic winds and fluxes associated with the NAO drive Ekman fluxes, anomalies in the strength of the intergyre gyre $\Psi_{\mathrm{ig}|w}$, and induce temperature differences between the two ocean boxes, δT_o, and hence anomalies in the overturning circulation, Ψ_{moc}. These result in anomalous ocean heat fluxes between the two ocean boxes, Q_o, inducing thermal anomalies, q, which in turn change the air–sea fluxes H, thermal radiation emitted to space I, temperature gradients in the atmosphere, δT_a, the atmospheric jet stream, and hence the surface winds.

Writing down the heat budget for each box, assuming that the storage of heat in the atmosphere is negligibly small, we obtain (see Fig. 7)

$$\frac{\partial q_N}{\partial t} = Q_o - Q_{\mathrm{ek}} - H_N, \tag{A1}$$

$$\frac{\partial q_S}{\partial t} = -Q_o + Q_{\mathrm{ek}} - H_S, \tag{A2}$$

$$H_N + Q_a = I_N, \tag{A3}$$

$$H_S - Q_a = I_S, \tag{A4}$$

where the subscripts N and S represent north and south,

respectively. It should be emphasized that no attempt is made here to represent the seasonal cycle or entrainment fluxes at the base of the ocean boxes—the model is perhaps best thought of as representing winter anomalies; see the discussion in section 5. All of the above quantities represent anomalies about their climatological values.

We are interested in the evolution of temperature *differences* across the diagonal of the Z because they can affect the overlying atmospheric jet stream. Thus differencing the two ocean boxes we obtain

$$\frac{\partial}{\partial t}\delta q = 2Q_o - 2Q_{\text{ek}} - \delta H, \tag{A5}$$

where $\delta(\ ) = (\ )_N - (\ )_S$.

Summing the two ocean boxes we find

$$\frac{\partial}{\partial t}(q_N + q_S) = -(H_N + H_S),$$

where $q_N + q_S$ is the change in total heat storage of the ocean within the Z as a whole and $(H_N + H_S)$ is the net air–sea flux over the Z. If we suppose that anomalies in air–sea interaction associated with the NAO are limited to the region straddled by the Z in Fig. 5, then since they have a dipole form (see Fig. 3a), we can assume that $H_N + H_S = I_N + I_S = 0$, where the *H's* are the anomalous air–sea heat fluxes, the shaded regions on either side of the diagonal of the Z. That this cancellation is realized in nature can be seen from Fig. 3b, where the oceanic heat flux implied by Fig. 3a is plotted. In NAO(+) the implied flux rises to a maximum at a latitude of 48°N but decreases to zero by the time 65°N has been reached. Thus, $H_N + H_S = 0$ and so, from the above, $(\partial/\partial t)(q_N + q_S) = 0$. Thus $q_N = -q_S$ and so

$$T_{oN} = -T_{oS}. \tag{A6}$$

Thus $\delta q = 2q_N$, $\delta H = 2H_N$, and (A5) just reduces to (A1); because of the asymmetry across the diagonal of the Z we need only consider either the northern or the southern boxes—the northern box is chosen for convenience. We now go on to consider the heat fluxes between the boxes.

Ocean heat fluxes: Gyre, thermohaline, and Ekman

The heat flux achieved by the intergyre gyre and by anomalies in overturning circulation are assumed to be given by (2) and (3), respectively.

Anomalous heat flux convergence due to Ekman layers is written thus:

$$Q_{\text{ek}} = c_o\overline{\Delta T}^{y}L_x\frac{\tau_{\text{nao}}}{f_o}, \tag{A7}$$

where τ_{nao} is the anomalous surface wind stress and $\overline{\Delta T}^{y}$ (>0) is the difference in SST averaged across the basin at latitudes corresponding to the horizontal lines of the Z (the DJF mean SST is plotted in Fig. 4a). We see that if the NAO is high, then $\tau_{\text{nao}} > 0$ and $Q_{\text{ek}} > 0$. Thus from (A1) and (A2), Ekman transport cools the ocean north of the diagonal of the Z and warms it south of the diagonal, as in Fig. 4a. Note that (A7) can be expressed as a pseudo air–sea heat flux by dividing it by the surface area of the box to yield a dipole pattern, just as seen in the observations in Fig. 4b.

We express the air–sea flux over the triangle of area

$$A = \frac{L_xL_y}{2} \tag{A8}$$

in terms of the air–sea temperature difference thus:

$$H_N = \lambda_{o,a}A\,(T_o - T_a)_N, \tag{A9}$$

where $\lambda_{o,a}$ is the linearized coefficient of combined latent and sensible heat flux.

Using (2), (3), (A7), and (A9), (A1) becomes, noting that $q_N = C_oAT_{oN}$:

$$C_oA\frac{\partial}{\partial t}T_{oN} = Q_M\Psi_m + Q_G\Psi_{g|w} - Q_E\tau - \lambda_{o,a}A(T_o - T_a)_N \tag{A10}$$

(which is the starting point for our discussion in section 3), where

$$Q_M = \rho_oc_o\overline{\Delta T}^{z} \times \Psi_M \tag{A11}$$

is a scale for heat transport due to thermohaline circulation,

$$\Psi_m = \frac{\Psi_{\text{moc}}}{\Psi_M} \tag{A12}$$

is a nondimensional measure of the strength of the anomalous overturning circulation with respect to the scale Ψ_M,

$$Q_G = \rho_oc_o\overline{\Delta T}^{\text{zero curl}} \times \Psi_G \tag{A13}$$

$$\Psi_g = \frac{\Psi_{\text{ig}}}{\Psi_G} \tag{A14}$$

are analogous quantities for gyre circulation,

$$Q_E = c_o\overline{\Delta T}^{y}L_x\frac{\tau_{\text{wind}}}{f_o} \tag{A15}$$

is a scale for Ekman heat transport,

$$\tau = \frac{\tau_{\text{nao}}}{\tau_{\text{wind}}} \tag{A16}$$

is a nondimensional measure of the surface wind stress with respect to the scale τ_{wind}, and

$$C_o = \rho_oc_oh \tag{A17}$$

is the heat capacity of the top h meters of ocean.

It should be emphasized that Eq. (A10) is expressed in terms of T_{oN} but, in view of (A6), the same equation (but with reversed signs) governs the evolution of T_{oS}.

Thus T_{oN} (or T_{oS}) is also telling us about the evolution of the north–south temperature difference across the diagonal—those gradients can be induced by Ekman heat transport, ocean gyres, thermohaline circulation, and stochastic air–sea heat flux.

We now go on to discuss the dynamics that control Ψ_m and $\Psi_{g|w}$ in (A10).

b. Incorporating dynamics

1) THE INTERGYRE GYRE

We suppose that changes in wind stress induce changes in the strength of Ψ_{ig} via the communication of linear oceanic baroclinic Rossby waves in a flat-bottomed ocean with an eastern boundary across which there can be no normal flow, just as in, for example, Frankignoul et al. (1997):

$$-\frac{\partial}{\partial t}\Psi_{\text{ig}} + c_R\frac{\partial \Psi_{\text{ig}}}{\partial x} = L_\rho^2 f_o w_{e_{\text{nao}}}, \tag{A18}$$

where $\Psi_{\text{ig}} = h\varphi$ with h a baroclinic depth scale and φ represents changes in the (first baroclinic mode) streamfunction, f_o is the Coriolis parameter and

$$c_R = \beta L_\rho^2 \tag{A19}$$

is the zonal phase speed of long, nondispersive Rossby waves with L_ρ the oceanic deformation radius, and w_e is the Ekman pumping velocity. Note that only the baroclinic response of the ocean is considered. We suppose that the gyre's heat transport is accomplished primarily by advecting the mixed layer temperature; if the upper-layer of a two-layer model is thin, then the baroclinic velocities in the upper layer will be much larger than the barotropic velocities, and so accomplish most of the transport.

The north–south extent of the domain, L_y, is set by that of the Z—that is, it is bounded by the horizontal zero-curl lines *of the anomaly*, a distance L_y apart (see Figs. 1b and 5). The eastern boundary is at $x = 0$ and the east–west extent of the basin is L_x, see Fig. 7b.

We write

$$\tau_{\text{nao}} = -\tau_{\text{wind}}\cos\left(\frac{\pi y}{L_y}\right) \tag{A20}$$

for the zonal component of the NAO(+) wind anomaly, varying as sketched in Fig. 8b, and capturing the essence of the observations (Fig. 2a). Thus

$$w_{e_{\text{nao}}} = -\frac{\tau_{\text{wind}}}{\rho_o f_o}\frac{\pi}{L_y}\sin\left(\frac{\pi y}{L_y}\right)$$

and is of one sign in the region straddled by the Z—as sketched in Fig. 5.

Substituting the above into (A18) and rearranging we obtain

$$-\frac{\partial}{\partial t}\Psi_g + c_R\frac{\partial}{\partial x}\Psi_g = -\tau\frac{c_R}{L_x}\sin\left(\frac{\pi y}{L_y}\right), \tag{A21}$$

where Ψ_g is given by (A14) and τ by (A16). Note that to derive the above we have divided (A18) through by the scale Ψ_G that appears in eq (A14), and set that scale to be

$$\Psi_G = \frac{L_x \pi \tau_{\text{wind}}}{\rho_o L_y \beta}, \tag{A22}$$

the transport of a gyre in Sverdrup balance on a β plane driven by a wind of strength τ_{wind} of the form (A20).

We suppose that

$$\tau = \frac{\tau_{\text{stochastic}} + \tau_{\text{SST}}}{\tau_{\text{wind}}} \tag{A23}$$

is made up of a stochastic, white noise component, representing the high-frequency, stochastic element of the NAO acting on the ocean and a component τ_{SST}, which is the feedback of SST on the NAO wind stress. Here $\tau_{\text{stochastic}}$ is independent of SST anomalies, τ_{SST} depends on SST anomalies. Unlike here, Neelin and Weng (1999) also consider stochastic forcing whose probability density function depends on SST. Note that stochastic and SST-dependent stress are assumed to have the same spatial form—that given in (A20) and sketched in Fig. 7—but have different temporal behavior.

As shown by Frankignoul et al. (1997), an ocean governed by Eq. (A21) with $\tau_{\text{SST}} = 0$, responds to imposed stochastic forcing in a ''red'' manner. For example, the time series of intergyre gyre transport, $\Psi_{g|w} = \Psi_g(x = -L_x)$ and heat flux, $Q_{\text{ig}} = \Psi_{g|w}Q_G$, shown in Fig. 8a is obtained by integrating Eq. (A21) forward—using MATLAB—assuming a white noise forcing (details are given in section 4). There is a flattening of the spectrum at frequencies lower that that associated with the time taken for Rossby waves to propagate across the basin—we solved for the spectrum of variability analytically in section 4.

This, then is our model of $\Psi_{g|w}$, in Eq. (A10). We now go on to discuss the dynamics governing Ψ_m.

2) THERMOHALINE CIRCULATION

The dynamics that govern the time-dependent thermohaline circulation are poorly understood (see discussion in section 4c). Provisionally we suppose, by analogy with the equation describing the overturning of a nonrotating fluid under the action of gravity, that

$$-\frac{1}{L_z^2}\frac{\partial}{\partial t}\Phi = \frac{g^*\alpha}{L_y}\delta T_o,$$

where g^* is an ''effective'' g acting on horizontal temperature gradients, Φ is the anomaly in the overturning streamfunction, L_z is its vertical scale, and α is the thermal expansion coefficient of water.

Noting that Ψ_{moc} ($\text{m}^3\ \text{s}^{-1}$) is $\Psi_{\text{moc}} = L_x\Phi$, where L_x

is the east–west scale, we multiply through by L_x and rearrange the above to obtain, using (A6):

$$\frac{\partial}{\partial t}\Psi_m = -ST_{oN}, \tag{A24}$$

where

$$S = \frac{2g^*\alpha L_z^2 L_x}{\Psi_M L_y}$$

is a ''solenoid'' term and Ψ_m is defined in (A12). Stochastic forcing of the thermodynamic equation (A10) will induce temperature gradients, which in turn drive thermohaline circulation: if $T_{oN} < 0$ then a positive thermohaline circulation anomaly, $\Psi_m > 0$, will be induced with enhanced sinking to the north.

Equation (A24) should be regarded as a ''place holder.'' The implications of different formulations are discussed in section 4c. Note that although (A24) does not yet include a frictional term, we nevertheless expect to find damped oscillatory solutions when it is coupled with (A10) and Ekman and gyre terms are set to zero.

c. Coupling assumptions

Equations (A10), (A21), and (A24) form a coupled system, provided that we can express $\tau_{\rm SST}$, the feedback of SST on surface winds in (A23), and T_{aN} in (A9) in terms of T_{oN}.

We do not attempt to develop a mechanistic model of the feedback of SST on surface winds—but see Cessi (2000). Instead we simply write

$$\frac{\tau_{\rm SST}}{\tau_{\rm wind}} = -f\frac{T_{oN}}{\Upsilon}, \tag{A25}$$

where f is a constant that maps T_{oN} onto $\tau_{\rm SST}$. Here Υ is a typical magnitude of the SST anomalies. We choose f to be a *positive* constant so that if $T_{oN} < 0$, corresponding to colder water in the northern triangle of the Z and warmer waters to the south, then $\tau_{\rm SST} > 0$, with stronger winds, a positive NAO and the jet stream shifted poleward of its climatological position, as in Fig. 2a. Conversely if $T_{oN} > 0$ then the above yields NAO(−) and a jet stream that has shifted southward.

Clearly (A25) is a simple parameterization of a very complex and incompletely understood chain of events in which synoptic-scale atmospheric eddies play a central role. We imagine that enhanced low-level baroclinity associated with enhanced SST gradients across and beneath the atmospheric jet stream, increases wave activity in the Atlantic storm track and hence the efficiency with which synoptic eddies transport westerly momentum into midlatitudes. Enhanced upper-level momentum transport projects efficiently onto the equivalent barotropic structure of the NAO and can readily excite it, ''bringing'' the upper-level westerlies down to the surface. Such a response has been observed in general circulation models of the atmosphere driven by dipoles in SST anomalies. For example, analysis of the ECHAM 2 AGCM driven by interannual SST forcing is presented by Neelin and Weng (1999, see their Fig. 2) and supports the simple representation (A25): dipole SST forcing in the North Atlantic with warm to the north and cold to the south induces a westward wind stress anomaly suggesting that $f > 0$. Figure 3 of Rodwell et al. (1999) shows the response of the Hadley Center model to NAO SST tripole forcing, again suggesting that f in (A25) is positive.[A1] Finally, connections between $\tau_{\rm SST}$ and SST can also be deduced from observations (but, because NAO $\leftrightharpoons$ SST, somewhat more ambiguously with respect to cause and effect)—see, for example, Deser and Blackmon (1993)—and again suggesting that f is positive.

To obtain a relationship between T_{aN} and T_{oN} we rearrange (A3) thus:

$$Q_a = -\lambda_{o,a}A(T_o - T_a)_N + BAT_{oN},$$

where we have used (A9) for the air–sea flux; set

$$I_N = BT_{N_{\rm SST}}A, \tag{A26}$$

where B is a radiative constant (see Simmonds and Chidzey 1982); and equated $T_{N_{\rm SST}}$ with T_{oN}. But, supposing that $Q_a = -(\delta T_{aN}/|\Delta T_a|)\overline{Q_a}$, where $\overline{Q_a}$ is the mean poleward heat transport across the jet stream in the mean and $|\Delta T_a|$ is the temperature change across the atmospheric jet stream in the mean, the above can be rearranged to yield our sought-after relationship between T_{aN} and T_{oN}:

$$T^{aN} = \eta T_{oN},$$

where

$$\eta = \frac{\left(1 - \frac{B}{\lambda_o}\right)}{\left(1 + \frac{2\overline{Q_a}}{|\Delta T_a|\lambda_o A}\right)}. \tag{A27}$$

We will see in appendix section d(2) that η is positive and about 1/2.

Finally, the air–sea temperature difference is

$$(T_o - T_a)_N = (1 - \eta)T_{oN}, \tag{A28}$$

expressing the fact that the atmosphere warms up over a warm SST anomaly, reducing the air–sea flux.

d. The coupled system

1) NONDIMENSIONAL EQUATIONS

The system—(A10), (A21), (A24)—together with the coupling relationships (A25) and (A28) may be written

[A1] Note, however, that R. T. Sutton (2000, personal communication) argues—but using a different version of the Hadley Center model than that employed by Rodwell et al. (1999)—that the southernmost lobe of the SST tripole in Fig. 2b is the primary NAO excitation mechanism, rather than the dipole straddling the Gulf Stream being invoked here.

for the gravest meridional mode in the following nondimensional form, where x has been nondimensionalized with respect to L_x, time with respect to $t_{\text{delay}} = L_x/c_R$, and temperature with respect to Υ:

$$\frac{\partial}{\partial t}T = m\Psi_m + g\Psi_{g|w} - \lambda T + F_T, \quad \text{(A29)}$$

$$-\frac{\partial}{\partial t}\Psi_g + \frac{\partial}{\partial x}\Psi_g = -\tau, \quad \text{(A30)}$$

$$\frac{\partial}{\partial t}\Psi_m = -sT, \quad \text{(A31)}$$

$$\tau = F_\tau - fT, \quad \text{(A32)}$$

where F_T, F_τ are stochastic forcing terms, for T and τ, respectively,

$$g = \frac{Q_G}{A\Upsilon}\frac{t_{\text{delay}}}{C_o} \quad \text{and} \quad \text{(A33)}$$

$$m = \frac{Q_M}{A\Upsilon}\frac{t_{\text{delay}}}{C_o}. \quad \text{(A34)}$$

The temperature in the northern ocean box, nondimensionalized with respect to Υ, is

$$T = \frac{T_{oN}}{\Upsilon} \quad \text{(A35)}$$

and the damping of ocean temperature anomalies by air–sea interaction is controlled by

$$\lambda = d - fe, \quad \text{(A36)}$$

where

$$d = \lambda_o\frac{t_{\text{delay}}}{C_o} \quad \text{(A37)}$$

with

$$\lambda_o = \lambda_{o,a}(1 - \eta) \quad \text{(A38)}$$

the damping coefficient for ocean temperature anomalies and

$$e = \frac{H_{ek}}{\Upsilon}\frac{t_{\text{delay}}}{C_o} \quad \text{(A39)}$$

represents the positive feedback of Ekman layers on T, where

$$H_{ek} = \frac{Q_E}{A} = 2\frac{c_o\overline{\Delta T}^y}{L_y}\frac{\tau_{\text{wind}}}{f_o} \quad \text{(A40)}$$

using (A15) and (A8) to yield a discrete version of (1).

The feedback of SST on the wind (A25) has been written

$$\frac{\tau_{\text{SST}}}{\tau_{\text{wind}}} = -fT \quad \text{(A41)}$$

and combined with (A23) to yield (A32).

Finally, the solenoid term driving meridional overturning is

$$s = S\Upsilon t_{\text{delay}}. \quad \text{(A42)}$$

In (A29) $\rightarrow$ (A32), all variables are nondimensionalized and the constants m (for meridional overturning), g (gyre), d (damping), e (Ekman), f (feedback), and s (solenoid) are dimensionless.

2) NUMERICAL ESTIMATES

If $L_x = 3000$ km and $c_R = 2$ cm s^{-1}, appropriate if the delay is governed by first baroclinic mode Rossby waves, then our unit of time is $t_{\text{delay}} = 1.5 \times 10^8$ s or, roughly, 4 yr. In these units a period of 8 yr corresponds to a nondimensional frequency of $\omega = \pi$.

Our scale for gyral heat transport is Q_G, Eq. (A13)—the heat transport of a gyre of strength Ψ_G crossing a mean temperature field with zonal temperature difference $\overline{\Delta T}^{\text{zerocurl}}$. If $\tau_{\text{wind}} = 0.05$ N m^{-2}, $L_x = L_y = 3000$ km, $\beta = 1.6 \times 10^{-11}$ s^{-1}, then Ψ_G, Eq. (A22), is 10 Sv. Setting $\overline{\Delta T}^{\text{zerocurl}} = 6°$C, a rough estimate of the change in ΔT along the climatological zero-curl line—see Fig. 4a—then $Q_G = 1/4$ PW [see discussion in section 2c(1)].

We set our scale for thermohaline heat transport, Eq. (A11), to be $Q_M = 1/2$ PW, appropriate if $\Psi_M = 15$ Sv and $\overline{\Delta T}^z = 8°$C (see section 2d).

The surface area occupied by 1/2 of the Z is $A = (3000 \text{ km} \times 3000 \text{ km})/2 = 4.5 \times 10^{12}$ m^2. The heat capacity of the upper 200 m of this ''triangle'' of ocean is $\rho_o c_o hA = 10^3 \times 410^3 \times 200 \times 4.5 \times 10^{12} = 3.6 \times 10^{21}$ J K^{-1}.

With the above choices we obtain, setting $\Upsilon = 1$ K:

$$g \simeq 10 \quad \text{(A43)}$$

$$m \simeq 20. \quad \text{(A44)}$$

One can physically interpret these numbers by inspection of (A33) and (A34): for example, g^{-1} is a measure of the time (in units of t_{delay}) for the intergyre gyre, transporting heat at rate Q_G (which would be achieved if $\Psi_{g|w} = 1$) to change the temperature of the ocean in one of the triangles of the Z by $\Upsilon = 1$ K.

The other timescale of interest is that due to air–sea interaction and is controlled by the parameter λ—Eq. (A36)—which depends on d, e, and f.

If λ_o, Eq. (A38), is $\lambda_o = 20$ W m^{-2} K^{-1}, as suggested by the observations[A2] analyzed by Frankignoul et al. (1997), then

[A2] Estimates of λ_o given in Frankignoul et al. (1997) already include the factor $(1 - \eta)$ in Eq. (A38), obviating the need for an independent estimate of η. However we note that because $B/\lambda_o \ll 1$ ($B = 2$ W m^{-2} K^{-1} as compared with $\lambda_o = 20$ W m^{-2} K^{-1}) and $2\overline{Q_o}/|\Delta T_a|\lambda_o A \sim 1$ (as deduced from a consideration of mean atmospheric heat balance), then Eq. (A27) suggests that $\eta \sim 1/2$.

$$d \simeq 3.5. \tag{A45}$$

If $\overline{\Delta T}^{y}$ 10 K (see Fig. 4a), Ekman processes have a magnitude of

$$e \cong 2.5 \tag{A46}$$

and so, depending on the magnitude of f, can be a nonnegligible countereffect to d.

A feedback of SST on wind stress of magnitude:

$$f \simeq \frac{1}{5} \tag{A47}$$

implies, from (A41), a τ_{SST} of 0.005 N m^{-2} if the SST dipole has magnitude $\sim\pm 1/2$ K and τ_{wind} in Eq. (A20) is 0.05 N m^{-2}. This is a modest feedback when compared to the magnitude of the NAO(+) wind stress anomaly plotted in Fig. 2a. The ECHAM 2 model results presented in Fig. 2 of Neelin and Weng (1999) show that a dipole anomaly of approximately ± 0.6 K induces a $\tau_{\mathrm{SST}} \sim 0.01$ N m^{-2} suggesting that $f \sim 0.4$. Indeed we showed in section 4b(c) that f must reach ~ 0.4 if the unforced coupled system is to exhibit (weakly damped or growing) oscillatory solutions, rather than strongly damped modes.

If $f \approx 0.4$, the above values of d and e yield:

$$\lambda \cong 2.5 \tag{A48}$$

implying, in dimensional terms, that air–sea interaction will damp a thermal anomaly of 1 K and depth 200 m with an e-folding timescale of ~ 1.6 yr.

Estimates of s are rather problematical and cannot be deduced directly from observations. But its rough size can be inferred from numerical experiments: Delworth (personal communication) and C. Herbaut (2000, personal communication) both observe fluctuations in modeled North Atlantic overturning streamfunction of order 3 Sv on timescales of a few years in ocean circulation models driven by NAO forcing. These fluctuations are associated with temperature anomalies of a degree or so. Thus if (nondimensionally) $\Psi_m \sim 1/5$ corresponds to a $T \sim 1$ on timescales of $t \sim 1$, then (A31) suggests that:

$$s \simeq \frac{1}{5}. \tag{A49}$$

REFERENCES

Barsugli, J. J., and D. S. Battisti, 1998: The basic effects of atmosphere–ocean thermal coupling on middle-latitude variability. *J. Atmos. Sci.,* **55,** 477–493.

Battisti, D. S., and A. C. Hirst, 1989: Interannual variability in the tropical atmosphere/ocean system: Influence of the basic state, ocean geometry and non-linearity. *J. Atmos. Sci.*, **46,** 1687–1712.

——, U. S. Bhatt, and M. A. Alexander, 1995: A modeling study of the interannual variability of the North Atlantic Ocean. *J. Climate,* **8,** 3067–3083.

Bjerknes, J., 1964: Atlantic air–sea interaction. *Advances in Geophysics,* Vol. 10, Academic Press, 1–82.

Bretherton, C., and D. Battisti, 2000: An interpretation of the results from atmospheric general circulation models force by the time history of the observed sea surface temperature distribution. *Geophys. Res. Lett.,* **27,** 767–770.

Cayan, D. R., 1992: Latent and sensible heat flux anomalies over the oceans: Driving the sea surface temperature. *J. Phys. Oceanogr.,* **22,** 859–881.

Cessi, P., 2000: Thermal feedback on windstress as a contributing cause of climate variability. *J. Climate,* **13,** 232–244.

Curry, R. G., M. S. McCartney, and T. M. Joyce, 1998: Oceanic transport of subpolar climate signals to mid-depth subtropical waters. *Nature,* **391,** 575–577.

Czaja, A., and J. Marshall, 2000: On the interpretation of AGCM's response to prescribed time-varying SST anomalies. *Geophys. Res. Lett.,* **27,** 1927–1930.

Delworth, T. L., and R. J. Greatbatch, 2000: Multidecadal thermohaline circulation variability driven by atmospheric surface flux forcing. *J. Climate,* **13,** 1481–1495.

Deser, C., and M. L. Blackmon, 1993: Surface climate variations over the North Atlantic Ocean during winter: 1900–1989. *J. Climate,* **6,** 1743–1753.

Dickson, R., J. Lazier, J. Meinke, P. Rhines, and J. Swift, 1996: Long-term coordinated changes in the convective activity of the North Atlantic. *Progress in Oceanography,* Vol. 38, Pergamon Press, 241–295.

Frankignoul, C., and K. Hasselmann, 1977: Stochastic climate models. Part II: Application to sea-surface temperature variability and thermocline variability. *Tellus,* **29,** 289–305.

——, P. Muller, and E. Zorita, 1997: A simple model of the decadal response of the ocean to stochastic wind forcing. *J. Phys. Oceanogr.,* **27,** 1533–1546.

——, A. Czaja, and B. L'Heveder, 1998: Air–sea feedback in the North Atlantic and surface boundary conditions for ocean models. *J. Climate,* **11,** 2310–2324.

Goodman, J., and J. Marshall, 1999: A model of decadal middle-latitude atmosphere–ocean coupled modes. *J. Climate,* **12,** 621–641.

Green, J. S. A., 1970: Transfer properties of the large-scale eddies and the general circulation of the atmosphere. *Quart. J. Roy. Meteor. Soc.,* **96,** 157–185.

Griffies, S. M., and E. Tziperman, 1995: A linear thermohaline oscillator driven by stochastic atmospheric forcing. *J. Climate,* **8,** 2440–2453.

Grotzner, A., M. Latif, and T. P. Barnett, 1998: A decadal climate cycle in the North Atlantic Ocean as simulated by the ECHO coupled GCM. *J. Climate,* **11,** 831–847.

Hakkinen, S., 2000: Decadal air–sea interaction in the North Atlantic based on observations and modeling results. *J. Climate,* **13,** 1195–1219.

Hall, A., and S. Manabe, 1997: Can local linear stochastic theory explain sea surface temperature and salinity variability? *Climate Dyn.,* **13,** 167–180.

Halliwell, G., 1998: Simulation of North Atlantic decadal/multidecadal winter SST anomalies driven by basin-scale atmospheric circulation anomalies. *J. Phys. Oceanogr.,* **28,** 5–21.

Hansen, D. V., and H. Bezdek, 1996: On the nature of decadal anomalies in North Atlantic sea surface temperature. *J. Geophys. Res.,* **101,** 8749–8758.

Hasselman, K., 1976: Stochastic climate models. Part I: Theory. *Tellus,* **28,** 289–305.

Hurrell, J. W., 1995: Decadal trends in the North Atlantic oscillation: Regional temperatures and precipitation. *Science,* **269,** 676–679.

Jin, F.-F., 1997: A theory of interdecadal climate variability of the North Pacific Ocean–atmosphere system. *J. Climate,* **10,** 324–338.

Joyce, T. M., C. Deser, and M. Spall, 2000: The relation between decadal variability of subtropical mode water and the North Atlantic oscillation. *J. Climate,* **13,** 2550–2569.

Kawase, M., 1987: Establishment of deep ocean circulation driven by deep-water production. *J. Phys. Oceanogr.,* **17,** 2294–2317.

Kushnir, Y., and I. Held, 1996: Equilibrium atmospheric response to North Atlantic SST anomalies. *J. Climate,* **9,** 1208–1220.

Lab Sea Group, 1998: The Labrador Sea Deep Convection Experiment. *Bull. Amer. Meteor. Soc.,* **79,** 2033–2058.

Latif, M., and T. P. Barnett, 1994: Causes of decadal climate variability in the North Pacific/North Atlantic sector. *Science,* **266,** 634–637.

Luksch, U., 1996: Simulation of North Atlantic low-frequency SST variability. *J. Climate,* **9,** 2083–2092.

Mehta, V. M., M. J. Suarez, J. Manganello, and T. L. Delworth, 2000: Predictability of multiyear to decadal variations in the North Atlantic oscillation and associated Northern Hemisphere climate variations: 1959–1993. *Geophys. Res. Lett.,* **27,** 121–124.

Morotzke, J., and B. Klinger, 2000: The dynamics of equatorially asymmetric thermohaline circulations. *J. Phys. Oceanogr.,* **30,** 955–970.

Neelin, J. D., and W. Weng, 1999: Analytical prototypes for ocean–atmosphere interaction at midlatitudes. Part I: Coupled feedbacks as a sea surface temperature dependent stochastic process. *J. Climate,* **12,** 697–721.

Palmer, T. N., and Z. Sun, 1985: A modeling and observational study of the relationship between sea surface temperature anomalies in the northwest Atlantic and the atmospheric general circulation. *Quart. J. Roy. Meteor. Soc.,* **111,** 947–975.

Peng, S., W. A. Robinson, and M. P. Hoerling, 1997: The modeled atmospheric response to middle-latitude SST anomalies and its dependence on background circulation states. *J. Climate,* **10,** 971–987.

Rodwell, M. J., D. P. Rowell, and C. K. Folland, 1999: Oceanic forcing of the wintertime North Atlantic oscillation and European climate. *Nature,* **398,** 320–323.

Rogers, J. C., 1990: Patterns of low-frequency monthly sea level pressure variability (1899–1986) and associated wave cyclone frequencies. *J. Climate,* **3,** 1364–1379.

Rossby, C.-G., 1939: Relation between variations in the intensity of the zonal circulation of the atmosphere and the displacements of the semi-permanent centers of action. *J. Mar. Res.,* **2,** 38–55.

Saravanan, R., and J. C. McWilliams, 1998: Advective ocean–atmosphere interaction: An analytical stochastic model with implications for decadal variability. *J. Climate,* **11,** 165–188.

Selten, F. M., R. J. Haarsma, and J. D. Opsteegh, 1999: On the mechanism of North Atlantic decadal variability. *J. Climate,* **12,** 1956–1973.

Simmonds, I., and C. Chidzey, 1982: The parameterization of longwave flux in energy balance climate models. *J. Atmos. Sci.,* **39,** 2144–2151.

Suarez, M. J., and P. S. Schopf, 1988: A delayed action oscillator for ENSO. *J. Atmos. Sci.,* **45,** 3283–3287.

Sutton, R. T., and M. R. Allen, 1997: Decadal predictability of North Atlantic sea surface temperature and climate. *Nature,* **388,** 563–567.

Sverdrup, H., 1947: Wind-driven current in a baroclinic ocean; with application to the equatorial currents in the eastern Pacific. *Proc. Natl. Acad. Sci. U.S.,* **33,** 318–326.

Taylor, A. H., and J. A. Stephens, 1998: The North Atlantic oscillation and the latitude of the Gulf Stream. *Tellus,* **50A,** 134–142.

Timmerman, A., M. Latif, R. Voss, and A. Grotzner, 1998: Northern Hemispheric interdecadal variability: A coupled air–sea mode. *J. Climate,* **11,** 1906–1931.

Visbeck, M., H. Cullen, G. Krahmann, and N. Naik, 1998: An ocean model's response to North Atlantic oscillation like wind forcing. *Geophys. Res. Lett.,* **25,** 4521–4524.

Weng, W., and J. D. Neelin, 1998: On the role of ocean–atmosphere interaction in middle-latitude interdecadal variability. *Geophys. Res. Lett.,* **25,** 167–170.